Cell

Recent Expansion of the Telomeric Complex in Rodents: Two Distinct POT1 Proteins Protect Mouse Telomeres

Dirk Hockemeyer,[1] Jan-Peter Daniels,[1] Hiroyuki Takai,[1] and Titia de Lange[1,*]
[1] Laboratory for Cell Biology and Genetics, The Rockefeller University, 1230 York Avenue, New York, NY 10021, USA
*Contact: delange@mail.rockefeller.edu
DOI 10.1016/j.cell.2006.04.044

SUMMARY

Human telomeres are protected by shelterin, a complex that includes the POT1 single-stranded DNA binding protein. We found that mouse telomeres contain two POT1 paralogs, POT1a and POT1b, and we used conditional deletion to determine their function. Double-knockout cells showed that POT1a/b are required to prevent a DNA damage signal at chromosome ends, endoreduplication, and senescence. In contrast, POT1a/b were largely dispensable for repression of telomere fusions. Single knockouts and complementation experiments revealed that POT1a and POT1b have distinct functions. POT1a, but not POT1b, was required to repress a DNA damage signal at telomeres. Conversely, POT1b, but not POT1a, had the ability to regulate the amount of single-stranded DNA at the telomere terminus. We conclude that mouse telomeres require two distinct POT1 proteins whereas human telomeres have one. Such divergence is unprecedented in mammalian chromosome biology and has implications for modeling human telomere biology in mice.

INTRODUCTION

Genome integrity in mammals requires shelterin, a protein complex that associates with the telomeric TTAGGG repeat array, regulates telomere length, and protects chromosome ends (reviewed in (de Lange, 2005)). Shelterin contains two DNA binding factors, TRF1 and TRF2, which anchor the complex along the double-stranded telomeric repeat array and recruit the shelterin components TIN2, TPP1 and Rap1. The sixth partner in shelterin is the single-stranded TTAGGG repeat binding protein, POT1, which associates with telomeres through its interaction with TPP1. Shelterin is ubiquitous and abundant at telomeres throughout the cell cycle. TRF1, TRF2, TIN2, and Rap1 are essential in the mouse ((Celli and de Lange, 2005; Chiang et al., 2004; Karlseder et al., 2003); T.d.L. and M. van Overbeek, unpublished data). Here, we describe the phenotype of POT1-deficient mouse cells.

The protective function of shelterin and the fate of dysfunctional telomeres has been deduced from the phenotypes associated with deletion of mouse TRF2 and inhibition of human TRF2 with a dominant-negative allele (Celli and de Lange, 2005; van Steensel et al., 1998). When TRF2 is compromised, telomeres are recognized as sites of DNA damage and processed as if they represent double-strand breaks. DNA damage response factors accumulate at chromosome ends, and the ATM kinase signaling pathway is activated, leading to cell cycle arrest and apoptosis or senescence (Celli and de Lange, 2005; d'Adda di Fagagna et al., 2003; Karlseder et al., 1999; Takai et al., 2003). The dysfunctional telomeres become a substrate for the nonhomologous end-joining (NHEJ) pathway by which DNA ligase IV joins most of the chromosome ends, creating long trains of fused chromosomes (Celli and de Lange, 2005; Smogorzewska et al., 2002; van Steensel et al., 1998). The single-stranded telomeric overhang is attacked by an NHEJ-dependent processing step, whereas the rest of the telomeric DNA appears to remain intact, leading to the presence of TTAGGG repeats at the sites of chromosome-end fusion (Celli and de Lange, 2005; Zhu et al., 2003).

A model has been proposed for the repression of NHEJ at mammalian telomeres (Griffith et al., 1999; de Lange, 2005). This model is based on the observation that mammalian telomeres can occur in an altered configuration, the t-loop, in which the 3′ telomeric overhang is strand-invaded into the duplex part of the telomeres (de Lange, 2005; Griffith et al., 1999). Since the NHEJ pathway relies on the loading of the Ku70/80 heterodimer on free DNA ends, t-loops could block NHEJ from accessing the chromosome end. The speculation is that loss of TRF2 results in opening of the t-loop, thus exposing the chromosome ends to Ku70/80 and enabling NHEJ. TRF2 has been implicated in the formation of t-loops based on its ability to generate similar structures in model substrates in vitro (Stansel et al., 2001). However, the role of TRF2 in t-loop formation in vivo has not been tested. It is also not known whether the t-loop configuration occurs at all telomeres and persists throughout the cell cycle.

POT1 was discovered based on its sequence similarity to proteins from hypotrichous ciliates that bind to the short single-stranded protrusion of the abundant chromosome ends in their macronuclei (Baumann and Cech, 2001). These ciliate telomere terminus factors recognize the sequence of the telomeric overhang in the context of a 3′ end. Structural analysis of the Oxytricha telomeric protein (TEBPα/β) showed that the complex hides the 3′ terminus in a deep hydrophobic protein pocket, a configuration that is thought to protect telomeres from inappropriate attack by nucleases (Horvath et al., 1998). In agreement with this proposal, the fission yeast ortholog of TEBPα, POT1, is required for the protection of telomeres from rapid degradation (Baumann and Cech, 2001). The structure of its DNA binding domain showed that human POT1 might position the 3′ terminus of its 5′-TTAGGGTTAG-3′ binding site in a protein pocket, leading to the proposal that the protection of mammalian telomeres largely depends on POT1 (Lei et al., 2004). According to this model, the telomere deprotection phenotype of TRF2$^{-/-}$ cells could be due to loss of POT1, since POT1 loading is in part dependent on TRF2 (Loayza and de Lange, 2003). The prediction of this model is that POT1 deficiency will generate a telomere deprotection phenotype similar to the phenotype of TRF2 loss.

In order to address the phenotype of POT1 deficiency, we and others have used RNAi and overexpression of human POT1 mutant alleles that do not bind single-stranded DNA (Hockemeyer et al., 2005; Liu et al., 2004; Loayza and de Lange, 2003; Veldman et al., 2004; Yang et al., 2005; Ye et al., 2004). In both settings, telomere length became deregulated, leading to excessive addition of telomeric repeats by telomerase (Liu et al., 2004; Loayza and de Lange, 2003; Ye et al., 2004). POT1 depletion also changed the structure of the telomere terminus (Hockemeyer et al., 2005). The amount of single-stranded telomeric DNA was diminished and the 5′ telomere end was altered from its precise [CCCAAT]nC-5′ sequence to a random position. Knockdown of POT1 also resulted in a DNA damage response but the response was transient, unlike the phenotype of TRF2 loss, and did not cause cell cycle arrest in immortalized cells (Hockemeyer et al., 2005). Furthermore, POT1 knockdown failed to elicit the severe telomere fusion phenotype observed upon inhibition of TRF2. However, as these experiments involve a partial (<10-fold) reduction of POT1, the exact role of POT1 in telomere protection remained to be determined. Here, we use gene targeting in the mouse to address the function of mammalian POT1.

RESULTS

Two Distinct POT1 Proteins at Mouse Telomeres

The human genome contains only one gene with significant homology to the ciliate telomere terminus proteins (Baumann and Cech, 2001), and a single POT1 gene is present in the primate, dog, and cow genomes (Figures 1A, 1B, and Figure S1A in the Supplemental Data available with this article online). In contrast, we identified two POT1 orthologs (POT1a and POT1b) in the mouse and rat genomes (Figures 1A and 1B). Mouse POT1a and POT1b show 71%–75% amino acid identity to human POT1 and to each other (Figures S1B and S1C). The mouse POT1a locus on chromosome 6 is syntenic with the human POT1 locus on chromosome 7; POT1b is located on mouse chromosome 17. The most likely origin of the two rodent POT1 genes is a recent gene duplication (Figure 1B). Both POT1 mRNAs are represented in the EST databases (POT1a: AK036052; POT1b: XM_355022) and appeared ubiquitously expressed based on RT-PCR (Figure 1C). The embryonic expression pattern of POT1a was examined using mice derived from a gene-trap ES cell line containing a β-galactosidase-neo (GEO) fusion gene inserted after the 8th coding exon in the POT1a locus (POT1a^{8GEO}; Figure S1D and see below). Heterozygous POT1a$^{8GEO/+}$ E13.5 embryos had β-galactosidase activity in the developing tissues (Figure 1D), indicating (near) ubiquitous expression during embryonic development.

Both POT1 proteins were detectable in immunoblots of extracts from mouse embryo fibroblasts (MEFs), ES cells, and NIH3T3 cells (Figure 1E). Two anti-sera raised against POT1a peptides detected a protein of ~70 kDa apparent MW whose abundance was significantly reduced by shRNAs specific to POT1a. Similarly, two anti-sera raised to POT1b peptides reacted with a protein of ~75 kDa apparent MW, that was identified as POT1b based on shRNA knockdown. Immunoblots and immunoprecipitation experiments indicated that the POT1a and POT1b antibodies were specific to the respective POT1 proteins (Figure 1E and data not shown). Semiquantitative immunoblotting experiments using recombinant proteins as a standard suggested that POT1a and POT1b are expressed at similar levels (Figure S1E).

Indirect immunofluorescence (IF) for POT1a and POT1b revealed the punctuate nuclear pattern typical of telomeres and many of the POT1 sites coincided with TRF1 signals (Figure 1F). Telomeric localization was also observed for myc-tagged POT1a and POT1b (see below, Figure S3B). Furthermore, chromatin immunoprecipitation (ChIP) with POT1a and POT1b antibodies recovered approximately the same amount of telomeric DNA but no chromosome-internal sequences, confirming that both proteins are specifically associated with telomeres (Figures 1G and S1F, and data not shown). RNAi-mediated partial (~70%) depletion of POT1a or POT1b demonstrated the specificity of the antibodies used in these experiments (Figures 1G and S1F).

Lack of POT1a Results in Embryonic Lethality, whereas POT1b$^{STOP/STOP}$ Mice Are Viable and Fertile

Whereas ES cells and mice heterozygous for the gene-trap allele POT1a^{8GEO} had no apparent phenotype, intercrosses of POT1a$^{8GEO/+}$ mice failed to yield homozygous offspring (Figure 2). POT1a$^{8GEO/8GEO}$ blastocysts failed to yield ES cells and cultured E1.5–E3.5 embryos did not form an inner cell mass and died around E6.5 (data not

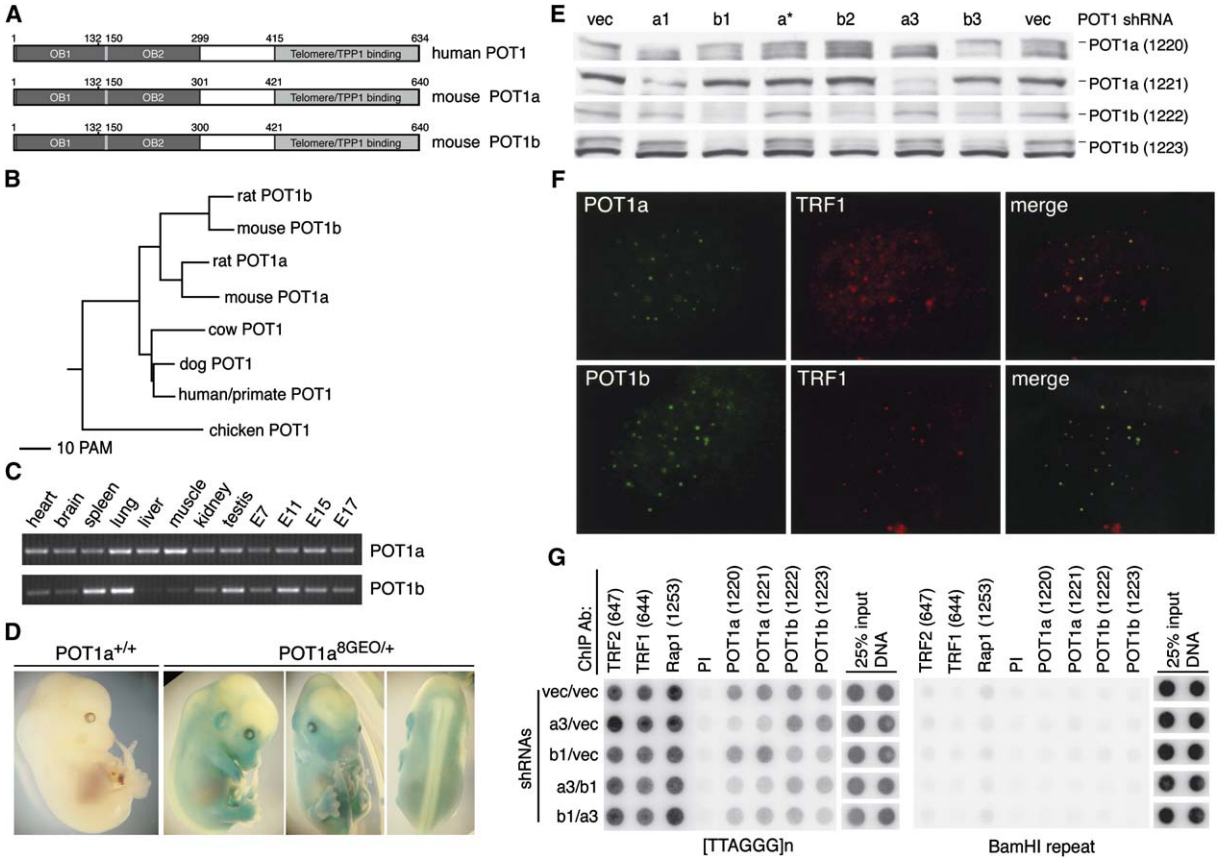

Figure 1. Two POT1 Proteins in the Mouse

(A) Schematic of the human and mouse POT1 proteins. Dark fill, OB folds; light fill, TPP1 interacting domain.

(B) Phylogenetic tree of vertebrate POT1 proteins based on the sequences given in Figure S1A using the Multalin website and default settings (http://prodes.toulouse.inra.fr/multalin/).

(C) Expression of POT1a and POT1b mRNAs in the indicated tissues and embryonic stages determined by RT-PCR.

(D) β-galactosidase staining of E13.5 embryos.

(E) Immunoblots for POT1a and POT1b on extracts from NIH3T3 cells with shRNAs to POT1a (a1 or a3) or POT1b (b1–b3). vec, vector control; a*, ineffective POT1a shRNA.

(F) IF for POT1a and POT1b in NIH 3T3 cells. IF with mouse anti-POT1a and POT1b sera (green) and rabbit anti-TRF1 (644) (red).

(G) Telomeric DNA ChIP for POT1a and POT1b. ChIPs with the indicated antibodies on NIH3T3 cells infected with shRNAs described in panel (E). Left: TTAGGG signal. Right: Bulk DNA detected with the BamHI repeat. For quantification, see Figure S1F.

shown). According to these data, POT1a is essential in early embryonic development and ES cells, even though POT1b is expressed (Figures 1C and 2E), suggesting that POT1a and POT1b are not redundant. We therefore generated mice carrying targeted alleles allowing conditional deletion of the third coding exon of POT1a, POT1b, or both. Analogous strategies were used for the POT1a and POT1b loci (Figures 2A and S2A); a detailed rationale for the targeting strategy is given in the Supplemental Data. The targeting construct introduced an FRT-flanked STOP cassette (Jackson et al., 2001) after the second coding exon, interrupting the first OB-fold of the DNA binding domain (Figure S1B). Cells heterozygous for the STOP allele showed ~50% less POT1a (or POT1b) protein (Figures 2E and 2G), consistent with previous data on the STOP cassette (Jackson et al., 2001). Intercrosses of POT1a$^{STOP/+}$ mice confirmed that POT1a deficiency is incompatible with mouse development (Figure 2C). However, POT1b$^{STOP/STOP}$ mice appeared healthy and fertile (Figures 2C and 2D). MEFs isolated from POT1b$^{STOP/STOP}$ embryos lacked POT1b (Figure 2E), and ChIP confirmed that POT1b was not present at telomeres whereas POT1a, TRF1, and TRF2 remained bound (Figure 2F).

The targeting strategy was such that floxed alleles of POT1a and POT1b could be generated allowing the isolation of MEFs from which the third protein coding exon (referred to as exon 3) of either gene could be deleted with Cre recombinase. Multiple independent POT1a$^{STOP/FLOX}$ and POT1b$^{STOP/FLOX}$ MEFs were isolated and immortalized with SV40 large T antigen (SV40-LT). Cre recombinase efficiently excised exon 3 as shown by PCR and RT-PCR and resulted in the expected loss of POT1a and

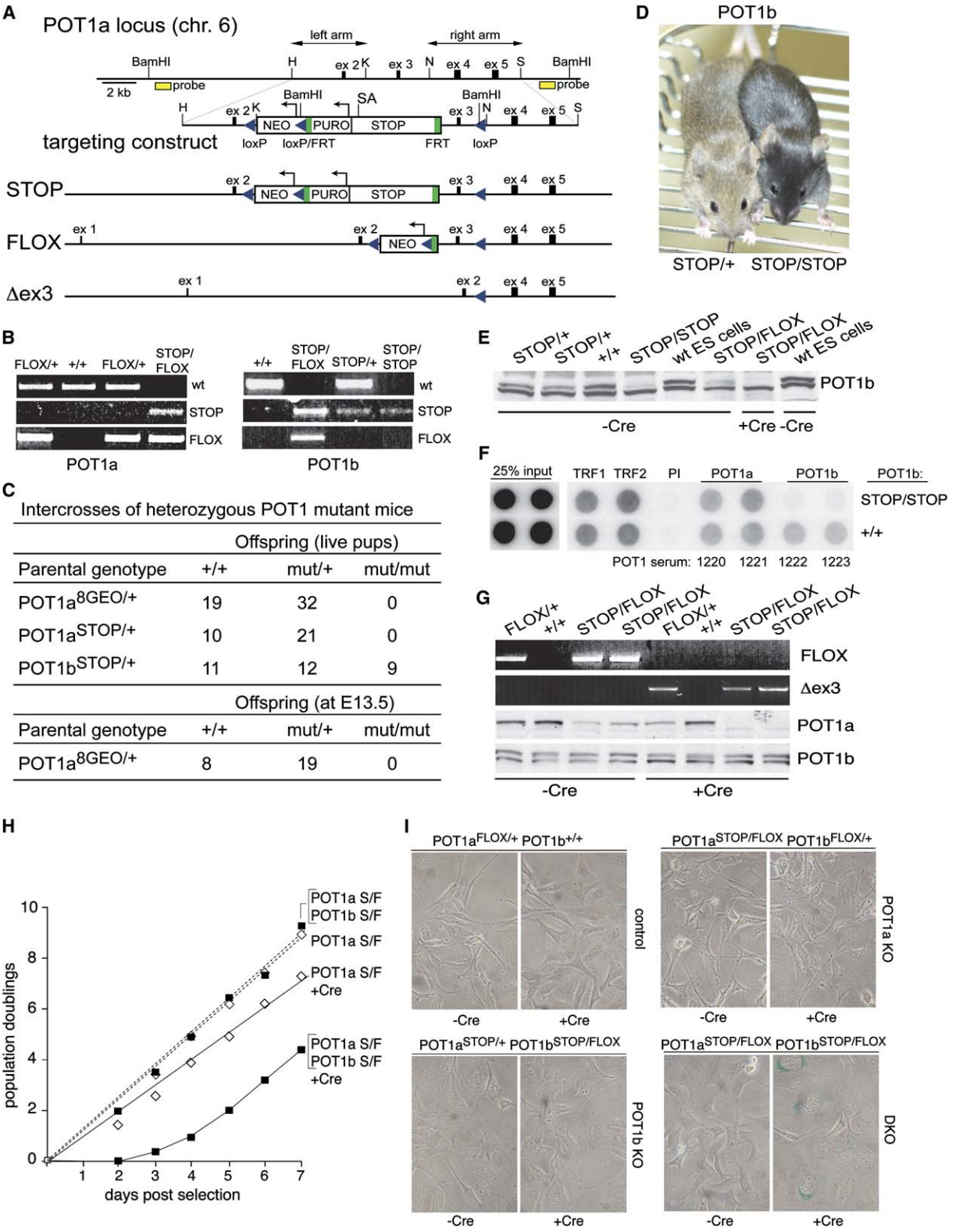

Figure 2. Conditional Deletion of POT1a and POT1b

(A) Targeting strategy for POT1a. Coding exons 1–5 of the POT1a genomic locus (chromosome 6), the targeting construct, and the POT1a alleles generated are shown. Yellow, probes used for genotyping (see Figure S2B); green boxes, FRT sites; blue, LoxP sites; SA, splice acceptor.

POT1b protein (Figures 2E, 2G, S2C, and S2D). Upon Cre-mediated deletion of either POT1 gene, the other POT1 paralog, TRF1, TRF2, and Rap1 remained associated with telomeres (see Figures 3 and 5 below and data not shown).

Redundant Roles for POT1a and POT1b in Cell Proliferation

Cre-mediated deletion of either POT1a or POT1b from SV40-LT immortalized MEFs did not lead to a growth arrest (Figure 2H and data not shown). Both cell types continued to proliferate with unaltered cellular morphology although POT1a-deficient cells grew slightly slower than the controls. Similarly, deletion of POT1a from primary MEFs did not result in a growth arrest (data not shown); POT1b deficiency is tolerated in the context of the whole animal, indicating that POT1b is also not required for proliferation of nontransformed cells. In contrast, simultaneous Cre-mediated deletion of POT1a and POT1b from $POT1a^{STOP/FLOX}POT1b^{STOP/FLOX}$ MEFs resulted in a rapid proliferative arrest (Figure 2H). These double-knockout (DKO) cells appeared to undergo senescence, as deduced from their enlarged and flattened morphology and their expression of SA-β-galactosidase (Figure 2I). The cultures were eventually overtaken by the small fraction of cells in which the Cre-mediated deletion of POT1a and/or POT1b was incomplete (Figure 2H and data not shown), hampering long-term analysis of DKO cells. $POT1a^{STOP/FLOX}POT1b^{STOP/FLOX}$ MEFs, which contain half the normal level of POT1a and POT1b, showed no growth defect (Figures 2H and 2I), nor did NIH3T3 cells in which POT1a and POT1b were simultaneously knocked down to ~30% with shRNA (data not shown). Thus, immortalized cells can proliferate normally without either POT1a or POT1b or when the total POT1 level is lowered 2- to 3-fold but not in the complete absence of both POT1a and POT1b.

Repression of the Telomere DNA Damage Signal by POT1a and POT1b

The role of POT1a and POT1b in the repression of the DNA damage signal at telomeres was assayed based on the formation of telomere dysfunction-induced foci (TIFs) (Takai et al., 2003), which are cytological foci of DNA damage response factors, such as 53BP1 and γ-H2AX, at chromosome ends. When both POT1a and POT1b were deleted, 70%–80% of the nuclei contained γ−H2AX and 53BP1 foci at most of the telomeres (Figures 3A–3C), indicating that the majority of chromosome ends had lost protection. Cells lacking only POT1b or cells heterozygous for POT1a and POT1b did not show this phenotype (Figures 3A, 3C, and S3A). A TIF response was also observed upon deletion of POT1a alone but the phenotype was limited to ~30% of the cells (Figures 3A and 3C), indicating that POT1b contributed to the protection of telomeres. The data suggest that POT1a is sufficient to repress DNA damage signaling at telomeres even when POT1b is absent. However, POT1b contributes to telomere protection and a complete telomere DNA damage response is only observed when both proteins are removed from the telomeres. DKO cells retained TRF2 and its interacting factor Rap1 at their telomeres (Figure 3D). Inspection of large numbers of nuclei before and after introduction of Cre showed no obvious change in the IF patterns and intensity of TRF2 and Rap1. In addition, there was widespread colocalization of TRF2/Rap1 signals with γ-H2AX in the DKO cells (Figure 3D). Thus, while TRF2 contributes to the recruitment of POT1 (Loayza and de Lange, 2003), POT1a/b are not needed for the accumulation of TRF2 and Rap1 at telomeres. Furthermore, the results indicate that telomeres lacking POT1a/b have lost the ability to prevent activation of a DNA damage signal, even though TRF2 is still present.

Whereas both POT1a and POT1b contribute to the repression of the DNA damage response at telomeres, the data suggested that POT1a and POT1b are not interchangeable in terms of this function. In order to further explore the possibility that POT1a and POT1b differ in their ability to repress the telomere DNA damage response, we monitored the ability of overexpressed myc-tagged POT1a and POT1b to repress the formation of TIFs in $POT1a^{-/-}$ cells. Both proteins were overexpressed and localized to telomeres (Figures 3F and S3B) but differed in their ability to protect the telomeres. Overexpression of POT1a diminished the frequency of TIF positive cells by 10-fold, whereas overexpression of POT1b had only a minor effect (Figure 3E). These data point to a functional difference between POT1a and POT1b and argue against the possibility that the distinct phenotypes of POT1a and

(B) Genotyping PCR for POT1a and POT1b using DNA from MEFs.
(C) Table of the genotypes found in the offspring of heterozygous intercrosses of indicated POT1a or POT1b mutant mice at weaning (top) or at E13.5 (bottom).
(D) Photograph of $POT1b^{STOP/+}$ (left) and $POT1b^{STOP/STOP}$ (right) mice.
(E) Immunoblot POT1b extracts from MEFs of the indicated genotypes and 129SV/J ES cells using antibody 1223 detecting POT1b (top band). For the +Cre lane, $POT1b^{STOP/FLOX}$ MEFs were infected with H&R-Cre virus and analyzed 5 days later.
(F) ChIP using the indicated antibodies on MEFs with the indicated genotype.
(G) Genotyping PCR and immunoblot analysis of POT1a mutant MEFs of the indicated genotype. Immunoblots with POT1a antibody 1221 and POT1b antibody 1223. Cells were infected with H&R-Cre virus were analyzed 5 days post infection (+Cre).
(H) Graph showing growth curves of SV40-LT immortalized MEFs targeted for either POT1a, or both POT1 genes after infection with pWZL-Cre or vector control viruses. Cells were selected with hygromycin for 96 hr, and proliferation was monitored over the next 7 days in medium without hygromycine. S/F, STOP/FLOX.
(I) Phase-contrast microscopic images of MEFs with the indicated genotypes with or without the infection with Cre adenovirus at 7 days after infection (stained for SA-β-galactosidase).

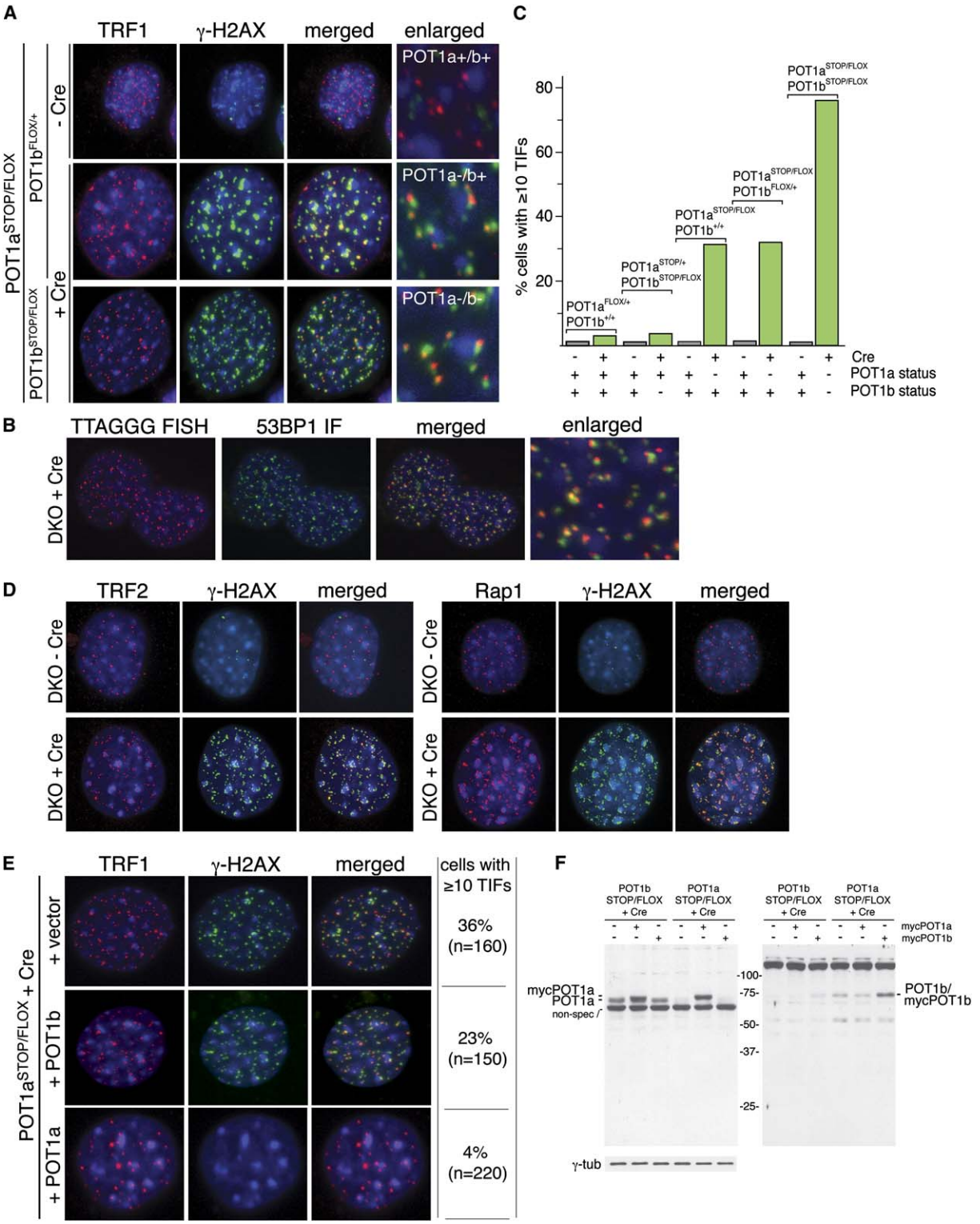

Figure 3. DNA Damage Signal at Telomeres Lacking POT1 Function

(A) MEFs of the indicated POT1 genotypes were infected either with pWZL-Cre retroviruses or control vector, selected for 5 days with hygromycine, and analyzed by IF for TRF1 (red), γ-H2AX (green), and counterstained with DAPI (blue).

(B) FISH-IF analysis of POT1 DKO cells treated as in (A), stained for telomeric DNA (red), 53BP1 (green), and DAPI (blue).

POT1b deletion are due to slight differences in the level of expression of the two genes.

Infrequent Chromosome-End Fusions in DKO Cells

Although many metaphases from the DKO cells showed no aberrations (Figure 4A, panel I), approximately 60% of the metaphases contained one or a few aberrant chromosomes (Figures 4A and 4B). Metaphase spreads in which telomeres were detected using FISH revealed the occurrence of chromosome-type fusions with telomeric DNA at the fusion site (Figure 4A, panels II–VI). These fusions affected ~2% of the chromosomes, which is 30-fold more frequent than in control cells (Figure 4B). The increase in fusions in DKO cells was significant and depended on the introduction of Cre (Figure 4B). However, the phenotype is much less pronounced than the nearly complete fusion phenotype of cells lacking TRF2 in which each chromosome undergoes one or two fusion events (Celli and de Lange, 2005). Furthermore, whereas TRF2 null cells have long trains of fused chromosomes, fusions of more than two chromosomes were rare in POT1 DKO cells (Figure 4A, panels II, III, and VI). The chromosome-type fusions occurred on both the short and long arm and in some cases clearly involved two different chromosomes (e.g., Figure 4A, panel IV). The fusions of two chromosomes always involved both chromatids, suggesting that most fusions occurred before DNA replication.

In addition to chromosome-type telomere fusions, DKO cells contained a significant number of chromosome fusions without detectable telomeric DNA at the fusion site (Figures 4A, panel IX, and 4B), which could be a consequence of breakage-fusion-bridge cycles. Consistent with this possibility, anaphase bridges were observed and occasionally, chromatin bridges containing telomeric signals persisted after reformation of the nuclear envelope (Figure 4A, panel X). DKO cells also contained a few complex chromosomal rearrangements as well as chromosomes with multiple TTAGGG repeat FISH signals separated by large segments of nontelomeric DNA (Figure 4A, panel IX). The origin of these rare abnormalities is not clear.

POT1 DKO cells appeared to have an unusual propensity to fuse or associate sister telomeres (Figures 4A, panels VII and VIII, and 4B). Although sister telomere fusions have been observed in cells lacking TRF2 (Smogorzewska et al., 2002), they are rare and the vast majority of fusions involve nonsister telomeres (Bailey et al., 2001). In order to distinguish sister telomere fusion from spurious juxtaposition, we only analyzed the q arm telomeres of chromosomes with clearly separated long arms. These long-arm sister telomeres of DKO cells showed a rate of sister fusion of ~1%–2% of the chromosomes per cell division which is comparable to the rate of nonsister fusions.

Each of the chromosomal abnormalities observed in DKO cells were also present in POT1a-deficient cells but at significantly reduced frequency (Figure 4B). In contrast, POT1b-deficient cells showed no increase in telomere fusions or other chromosomal abnormalities (Figure 4B). Thus, POT1a appears to be sufficient for the protection of telomeres from inappropriate fusion and in its absence POT1b can partially, but not fully compensate for this function. However, the telomere fusion phenotype of DKO cells is minor compared to the phenotype of TRF2$^{-/-}$ cells, indicating POT1 function is largely dispensable for the repression of NHEJ at telomeres.

Endoreduplication with Formation of Diplochromosomes

POT1a/b DKO cells displayed extensive endoreduplication (Figures 5 and S4). As a result, some of the DKO interphase nuclei had an increased size and contained supernumerary telomeric signals (see for example Figure 5A). In these nuclei, the telomeres tended to cluster around regions of more intense DAPI staining, which is expected since half of the mouse telomeres abut the centromeric heterochromatin. Metaphase spreads revealed a high frequency (~17%) of endoreduplicated karyotypes in which all chromosomes were present as diplo- or quadruplochromosomes (Figures 5B and S4B). Endoreduplication with formation of diplochromosomes is rare in immortalized control MEFs (≤3% of metaphases; Figures S4A and S4B). FACS analysis showed that POT1a/b DKO induced an increase in cells with 8N and 16N DNA content (Figures 5C and 5D), consistent with one and two rounds of endoreduplication, respectively.

The repression of endoreduplication by POT1 proteins followed the pattern seen for repression of the DNA damage signal and (rare) telomere fusions. POT1a-deficient cells exhibited endoreduplication with formation of diplochromosomes in approximately 17% of the metaphase spreads (Figure S4B). However, FACS analysis indicated that their extent of endoreduplication was somewhat less than the DKO cells and metaphases with quadruplochromosomes were not observed (Figure S4A and data not shown). FACS analysis and inspection of metaphase spreads showed that endoreduplication was not induced in POT1b-deficient cells (Figures S4A and S4B). Thus, also with regard to endoreduplication, POT1a is primarily responsible for repression of this phenotype. The mechanism

(C) Quantification of TIF-positive cells. Cells with 10 or more TRF1 signals colocalizing with γ−H2AX foci were scored, n ≥ 100. Gray bars, no Cre, control vector; green bars, pWZL-Cre.

(D) POT1a$^{STOP/FLOX}$ POT1b$^{STOP/FLOX}$ examined before and after Cre expression as in (A) but using antibodies to TRF2 (1254, red) or Rap1(1252, red) and γ-H2AX (green) for IF. The images of nuclei − Cre and + Cre are not shown at the same magnification. Cre-treated nuclei are considerably larger.

(E) Suppression of the DNA damage response in POT1a$^{-/-}$ cells by POT1a but not POT1b. POT1a$^{STOP/FLOX}$ cells were treated with Cre to delete POT1a and subsequently infected with retroviruses expressing N-terminally myc-tagged POT1a or POT1b (or the empty pLPC myc vector), as indicated. TIFs were detected and scored as in panels (A) and (C).

(F) Immunoblot detection of POT1a and POT1b overexpression in POT1a- or POT1b-deficient cells. Genotypes and overexpression as indicated above the lane. Myc-tagged POT1a migrates slightly slower than the endogenous POT1a.

A

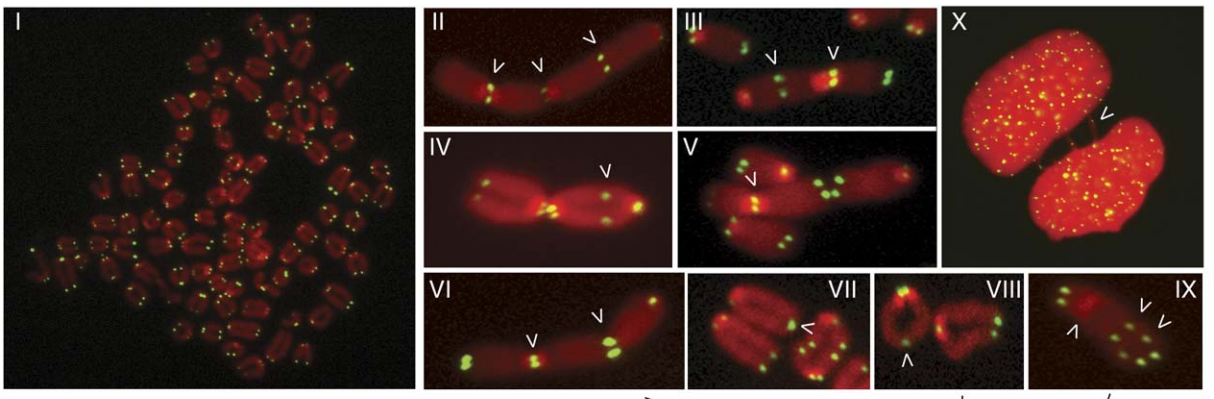

B

Genotype	Cre	POT1a status	POT1b status	Chromosomes analyzed	Chromosome fusions + tel. signal	Chromosome fusions - tel. signal	Sister fusions	Multiple tel. signals
POT1a$^{FLOX/+}$ POT1b$^{+/+}$	-	+/+	+/+	1851	2	3	0	1
	+	+/-	+/+	2171	1	4	0	0
POT1a$^{STOP/FLOX}$ POT1b$^{+/+}$	-	+/-	+/+	2023	1	2	0	0
	+	-/-	+/+	2318	6 (0.3%)	17 (0.7%)	15 (0.6%)	1
POT1a$^{STOP/+}$ POT1b$^{STOP/FLOX}$	-	+/-	+/-	2616	1	3	2	0
	+	+/-	-/-	2670	1	4	2	3
POT1a$^{STOP/FLOX}$ POT1b$^{STOP/FLOX}$	-	+/-	+/-	2773	2	5	0	0
	+	-/-	-/-	3485	69 (2%)	43 (1.2%)	49 (1.4%)	6

Figure 4. Mild Telomere Fusion Phenotype Associated with POT1 Deficiency

(A) Metaphase spreads of SV40-LT MEFs with telomeric DNA detected by FISH (green); DNA stained with DAPI (false-colored in red). POT1a$^{STOP/FLOX}$ POT1b$^{STOP/FLOX}$ MEFs were infected with AdCre and analyzed 78 hr later. Representative metaphase (I). Examples of the chromosomal aberrations found in the POT1 DKO: chromosome-type fusions with and without telomeric DNA at the site of fusion (II–VI), sister telomere fusions (VII–VIII), chromosomes with multiple internal TTAGGG signals (IX), and two nuclei connected with multiple chromatin bridges containing telomeric signals.

(B) Frequencies of aberrant chromosomes in metaphases (as in [A]) of POT1a- and/or POT1b-deficient MEFs. Fusions of short arm sister telomeres were not scored.

by which loss of POT1 function induces endoreduplication is not known. Chromosome-end fusions are not a likely culprit since they are thought to impede the progression of mitosis after resolution of the centromeric cohesin and hence do not explain the occurrence of diplochromosomes which retain cohesion at the centromeres.

POT1b Controls Telomerase-Independent Processing of the Telomere Terminus

The structure of the telomeres in cells lacking POT1a and/or POT1b was examined by genomic blotting of telomeric restriction fragments (Figures 6 and S5). Although each mouse embryo has a different pattern of telomeric restriction fragments, the size of the bulk telomeres can be assessed when the DNA is fractionated on CHEF gels. This analysis indicated that deletion of POT1a or POT1b did not result in a rapid loss or elongation of telomeric DNA. Furthermore, the size of the telomeric fragments of second-generation POT1b-deficient mice was unaltered (Figure 6C). In addition, DKO cells had telomeres in a normal size range, consistent with the retention of the telomeric FISH signals in interphase cells and metaphase spreads (Figures 3–5).

The status of the telomere terminus was examined by quantitative analysis of the 3′ telomeric overhang. The single-stranded telomeric DNA was detected in native

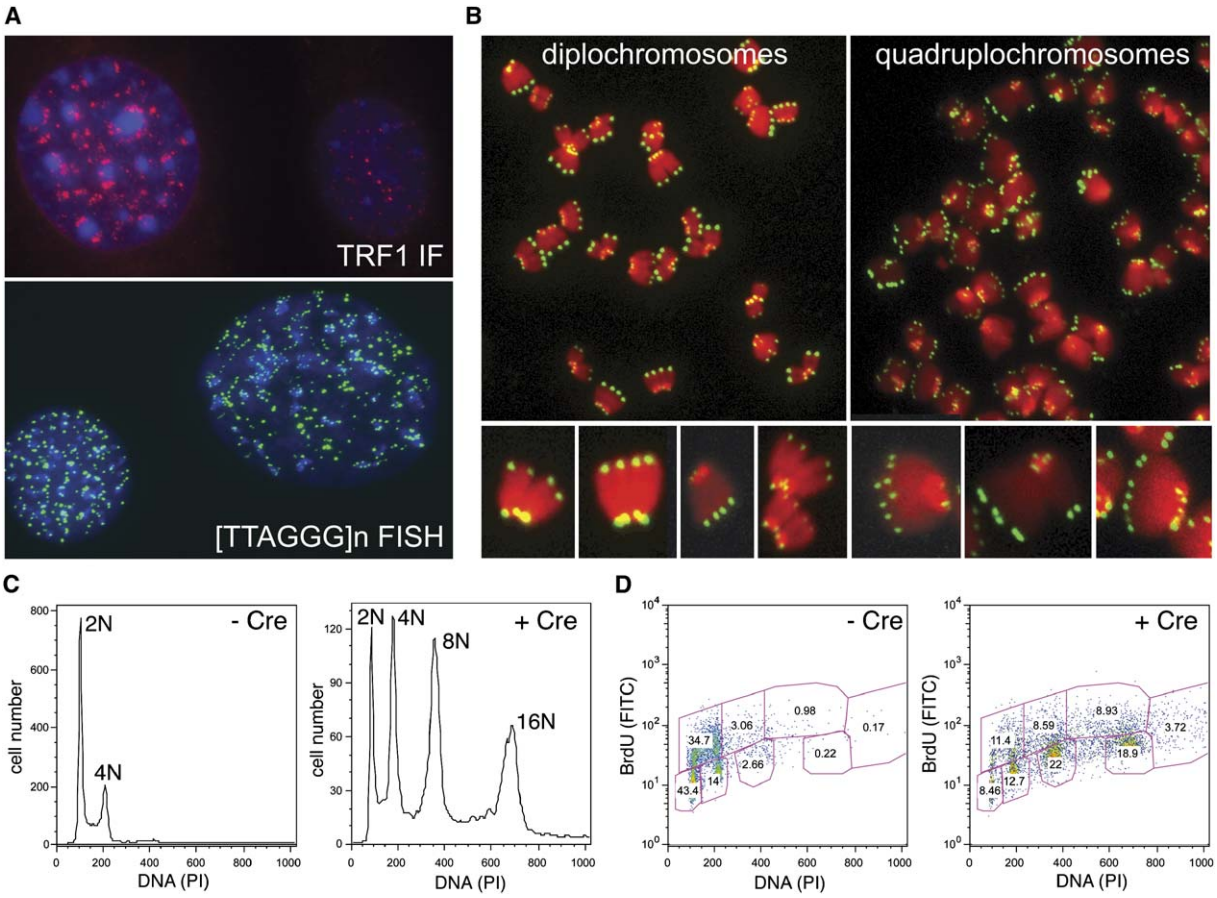

Figure 5. Endoreduplication with Diplo- and Quadruplochromosomes in DKO Cells

(A) Example of enlarged DKO nuclei with supernumerary telomeres. Top panel: TRF1 IF (red) in POT1 DKO cells counter stained with DAPI (blue). The nucleus on the left is enlarged and shows increased numbers of telomeric TRF1 foci and telomere clustering around heterochromatin. The nucleus on the right is of normal size. Bottom: Telomeric FISH (green) in DKO cells counter stained with DAPI (blue). Enlarged nucleus with supernumerary telomeres on the right shown next to a nucleus of normal size.

(B) Telomeric FISH on DKO metaphase chromosomes showing diplochromosomes and quadruplochromosomes.

(C) FACS profiles of POT1a$^{STOP/FLOX}$ POT1b$^{STOP/FLOX}$ MEFS infected with pWZL-Cre or vector control, selected for 5 days, and analyzed 2 days after selection. Sub-G1 cells are not shown.

(D) MEFs were treated as in (C) and incubated in BrdU for 1 hr prior to harvesting. FACS profiles represent BrdU content and DNA content. Numbers represent % of cells in each compartment.

DNA gels using a single-stranded [CCCTAA]4 probe. After quantification of the signal, the DNA was denatured in situ and the total amount of telomeric DNA was determined in the same lane by rehybridization with the [CCCTAA]4 probe. The ratios of single-stranded to total telomeric DNA signals were compared between samples in order to evaluate changes in the single-stranded TTAGGG repeat DNA. The relative amount of single-stranded TTAGGG repeats was not altered upon deletion of POT1a (Figures 6A, 6B, and S5). In contrast, loss of POT1b resulted in increased single-stranded telomeric DNA signals (Figures 6A and 6B). The increased signal was derived from a 3′ overhang since it was sensitive to the *E. coli* 3′ exonuclease ExoI (Figure S5A). POT1b$^{STOP/STOP}$ mice showed a 7- to 11-fold increase in the overhang signal in liver, kidney, and spleen, and this phenotype was stable over two generations (Figure 6C and data not shown). It appeared that the overhangs in POT1b-deficient MEFs gradually increased with proliferation (data not shown), consistent with the greater amount of ss TTAGGG DNA in vivo.

Cells lacking both POT1a and POT1b had a similar overhang extension phenotype as POT1b-deficient cells (Figures 6A, 6B, and S5). Due to the rapid arrest of the DKO cells, we could not determine whether POT1a loss exacerbates the phenotype. The DKO cells contained a class of overhang-bearing telomeric restriction fragments that migrated throughout the lane, suggesting an unusual DNA structure. The smearing of the signal into the higher MW fractions and beyond was not prominent when the total telomeric DNA was examined after denaturation of the DNA, indicating that these molecules were relatively rare and only detectable due to their longer overhangs.

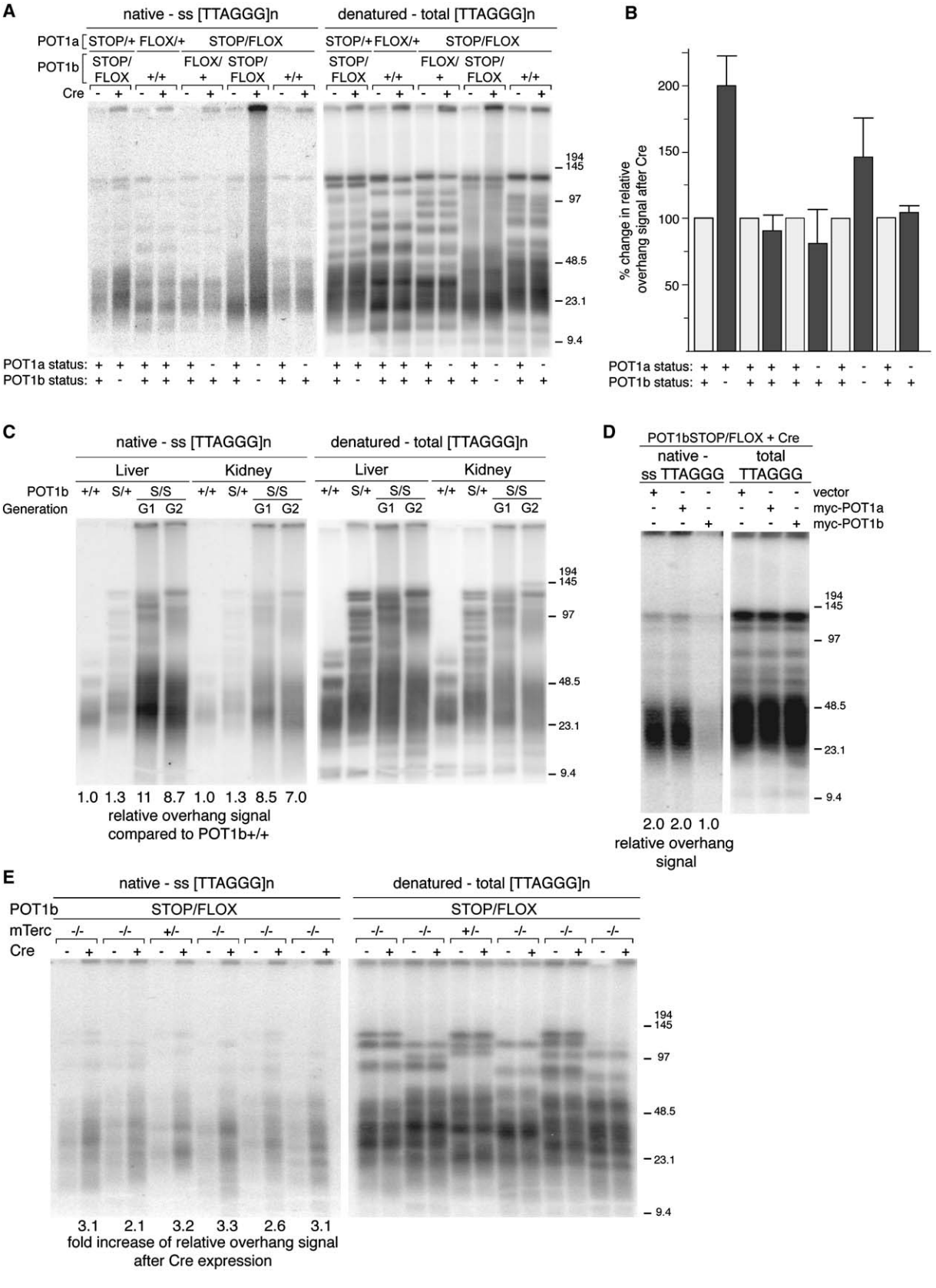
A
native - ss [TTAGGG]n
denatured - total [TTAGGG]n
POT1a
POT1b
STOP/+ FLOX/+ STOP/FLOX
STOP/ FLOX +/+ FLOX/ + STOP/ FLOX +/+
Cre
194
145
97
48.5
23.1
9.4
POT1a status: + + + + + - + - + -
POT1b status: + - + + + + + - + +
B
% change in relative overhang signal after Cre
200
150
100
50
POT1a status: + + + + + - + - + -
POT1b status: + - + + + + + - + +
C
native - ss [TTAGGG]n
denatured - total [TTAGGG]n
Liver
Kidney
POT1b +/+ S/+ S/S
Generation G1 G2
1.0 1.3 11 8.7 1.0 1.3 8.5 7.0
relative overhang signal
compared to POT1b+/+
D
POT1bSTOP/FLOX + Cre
native - ss TTAGGG
total TTAGGG
vector
myc-POT1a
myc-POT1b
2.0 2.0 1.0
relative overhang signal
E
native - ss [TTAGGG]n
denatured - total [TTAGGG]n
POT1b STOP/FLOX
mTerc -/- -/- +/- -/- -/- -/-
Cre
3.1 2.1 3.2 3.3 2.6 3.1
fold increase of relative overhang signal
after Cre expression

In order to establish whether the elongation of the overhangs was a specific phenotype of loss of POT1b, we determined to what extent exogenously expressed POT1a and POT1b were able to suppress this phenotype of POT1b-deficient cells. As shown above (Figures 3F and S3B), both proteins were overexpressed and localized to telomeres. POT1b was able to reestablish a normal telomere terminus structure, whereas POT1a overexpression had no effect (Figure 6D). We conclude that the control of the telomeric overhang is primarily dependent on POT1b.

We next asked whether the extended telomeric overhangs are due to deregulation of telomerase at the telomere terminus. POT1b mutant mice were crossed with mice that lack telomerase due to deletion of the mTERC gene encoding the RNA component of telomerase (Blasco et al., 1997). MEFs that lacked mTERC and had a conditional POT1b allele were established and immortalized with SV40-LT. Cre-mediated POT1b deletion resulted in comparable extension of the 3′ overhang in both mTERC$^{+/-}$ and mTERC$^{-/-}$ cells, indicating that telomerase is not responsible for the elongation of the 3′ ends (Figure 6E). We conclude that POT1b maintains the integrity of the telomere terminus by regulating a telomerase-independent processing step.

DISCUSSION

Our results reveal an unexpected difference between human and rodent shelterin. Human shelterin contains a single POT1 protein, whereas the mouse version of this complex is more elaborate, containing roughly equal levels of two functionally distinct POT1 proteins, POT1a and POT1b. Since their duplication, the two mouse POT1 paralogs diverged to the extent that full protection of the telomeres requires both factors. For example, POT1a is necessary to fully repress a DNA damage signal at telomeres. POT1b can partially compensate for the loss of POT1a, but its ability to repress the telomere damage response is incomplete. Conversely, POT1b has a specific role in regulating the structure of the telomere terminus, leading to deregulation of the telomeric overhang in POT1b-deficient cells, despite the presence of POT1a. Thus, while POT1a and POT1b are relatively recent additions to shelterin, they have distinct functions and are both required for the protection of mouse telomeres. It is possible that the single human POT1 protein combines the functions of mouse POT1a and POT1b although attempts at complementation with human POT1 have so far failed (D.H. and T.d.L., unpublished data).

Within the context of fundamental aspects of mammalian chromosome biology, the rodent duplication of the POT1 gene and functional divergence of the two resulting POT1 paralogs is unprecedented. No comparable case has emerged from comparisons of human and mouse genes involved in kinetochore function, origin firing and regulation, or DNA damage detection and repair. Other genes relevant to telomere biology, such as those for telomerase components and the genes for the other shelterin proteins are present at single copy in all sequenced mammalian genomes. Previous findings revealed substantial differences between the telomeric proteins in budding yeast on the one hand and fission yeast and mammals on the other. The current results provide evidence for much more recent changes in the telomeric complex and attest to the rapid evolution of the telomere/telomerase system.

POT1a and POT1b Play a Key Role in Repressing the Telomere DNA Damage Response

POT1a/b DKO cells lack the ability to distinguish telomeres from sites of DNA damage. Most of their telomeres become associated with DNA damage response factors and the cells arrest, most likely due to a permanent DNA damage signal. The severity of this telomere damage phenotype is similar to that of mouse cells lacking TRF2 (Celli and de Lange, 2005). Yet, TRF2 is not removed from telomeres lacking POT1a/b. This finding raises the possibility that the POT1 proteins contribute to the mechanism by which TRF2 prevents DNA damage signaling at chromosome ends (Figure 7). The recruitment of POT1 to telomeres is thought to depend on both TRF1 and TRF2, which bring the POT1 interacting factor TPP1 to the telomere (reviewed in de Lange, 2005). While these interactions have not been verified in mouse cells, the residues required for TPP1 binding are conserved in mouse POT1a and POT1b. Thus, the DNA damage phenotype of TRF2 null mouse cells could be solely due to insufficient

Figure 6. POT1b Controls a Telomerase-Independent Telomere Terminus Processing Step

(A) DNA from MEFs of the indicated genotypes were analyzed using the in-gel telomere overhang assay. Phenotypes were analyzed 7 days after infection with H&R-Cre or without infection at the same time point. The left image shows hybridization signal using the TelC probe ([CCCTAA]$_4$) under native conditions detecting the telomeric 3′ overhang. The right image shows the total telomeric hybridization signal obtained with the same probe after in-gel denaturation of the DNA. MEFs are derived from littermate embryos and were analyzed 1 week after introduction of Cre.

(B) Quantification of overhang changes based on three independent experiments as shown in (A). Bar graphs represent quantified overhang signals normalized to the total telomeric signal in the same lane. For each genotype, % overhang change induced by Cre are depicted. Error bars represent one SD.

(C) In-gel overhang assay of cells isolated from liver and kidney from mice with the indicated genotype. Left panel shows the native overhang signal, right panel shows the denatured total telomeric DNA. Relative overhang signals are indicated below the lanes. (D) Repression of the overhang phenotype by overexpression of POT1b, not POT1a. POT1b$^{STOP/+}$ or POT1b$^{STOP/FLOX}$ cells were treated with Cre and infected with retroviruses expressing myc-tagged POT1a or POT1b as shown in Figure 3F. Telomeric overhang signals were determined as in panel (A).

(E) In-gel overhang assay of MEFs either heterozygous or null for mTerc and conditionally targeted for POT1b with or without H&R-Cre infection. Left panel shows the native overhang signal, right panel shows the denatured total telomeric DNA. All MEFs are derived from littermates embryos. MEFs were examined 1 week after introduction of Cre. MEFs in lanes (from left) 3, 4, 5, 6, 9, and 10 were POT1a$^{FLOX/+}$.

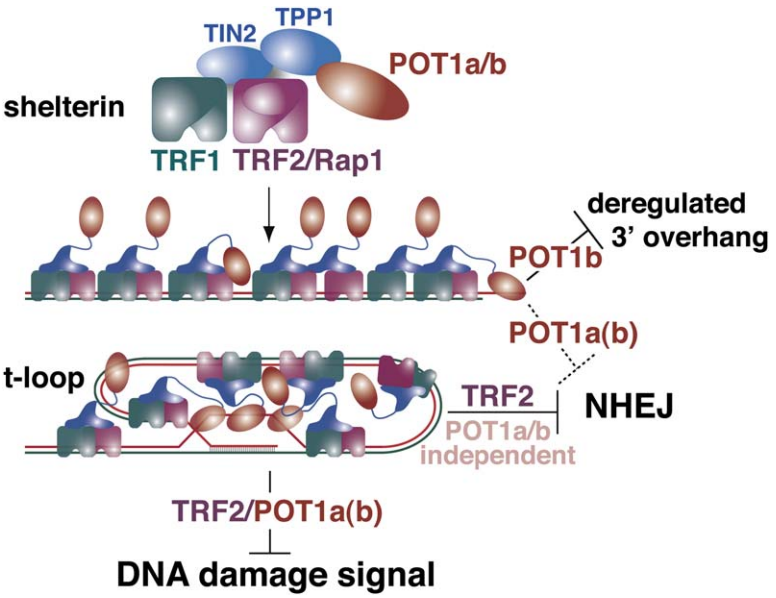

Figure 7. Summary of the Roles of TRF2, POT1a, and POT1b at Mouse Telomeres

Mouse shelterin is depicted as a complex of TRF1, TRF2, Rap1, TIN2, TPP1, and POT1a and POT1b. The details of the protein interactions are in part based on information from human shelterin. It is not known whether POT1a and POT1b are present in the same complex or in two different versions of shelterin. Repression of the DNA damage signal at telomeres requires TRF2, POT1a and POT1b. Repression of NHEJ is largely independent of POT1a and –b but requires TRF2. NHEJ is proposed to be repressed through sequestration of the telomere terminus in the t-loop. POT1a and POT1b are proposed to repress NHEJ at telomeres that are not in the t-loop configuration. POT1b is required to prevent generation of inappropriately long telomeric 3′ overhangs.

POT1 at the chromosome ends but other possibilities have not been excluded.

The Repression of NHEJ at Telomeres

When TRF2 is deleted, most telomeres are processed by the NHEJ pathway, leading to nearly complete fusion of the genome (Celli and de Lange, 2005). In contrast, telomeres lacking POT1a and POT1b remain largely protected from this type of inappropriate repair. This result indicates that POT1 is not required for the repression of most NHEJ events and is consistent with NHEJ being blocked by the formation of t-loops, a process ascribed to TRF2 (Figure 7). However, a small fraction of the chromosome ends in POT1 DKO cells do undergo fusions, pointing to an important, albeit minor role of POT1a/b in the repression of NHEJ. One possibility is that POT1a/b aids in repression of NHEJ when t-loops are resolved (Figure 7), for instance when the replication fork progresses through the strand-invasion site. We imagine that the presence of POT1a/b on the single-stranded overhang might interfere with efficient loading of Ku70/80 or prevent cleavage of the overhang, thereby thwarting NHEJ.

POT1b Blocks Formation of Excessive Single-Stranded Telomeric DNA

The maintenance of the normal structure of the telomere terminus is dependent on POT1b. In its absence, cells contain up to 10-fold more single-stranded TTAGGG repeat DNA. Although we do not know whether the increase in overhang sequences affects all telomere equally, if it does, the overhangs may be as long as 2 kb. The total amount of single-stranded TTAGGG repeat DNA could be in excess of 200 kb in the nuclei of liver cells lacking POT1b. This type of alteration has not previously been observed in mammalian cells, nor does it occur in fission yeast lacking POT1 (Baumann and Cech, 2001). However, in the budding yeast cdc13-1 mutant, inactivation of the POT1-like Cdc13 protein results in excessively long 3′ overhangs (Garvik et al., 1995). The long single-stranded regions are thought to activate the MEC1/RAD9 pathway, explaining the lethality of cdc13-1. In contrast, the excess single-stranded DNA of POT1b-deficient cells did not appear to activate a DNA damage checkpoint and mice lacking POT1b are healthy and fertile. In the cdc13-1 mutant, the long 3′ overhangs are generated by exonucleolytic degradation of the C-rich telomeric DNA strand in an Exo1- and Rad24-dependent manner (Zubko et al., 2004). A similar mechanism may well be responsible for the excess single-stranded telomeric DNA in POT1b-deficient cells (Figure 7). In this regard, RNAi-mediated knockdown of human POT1 results in an altered sequence at the 5′ end of the C-rich telomeric repeat strand which could also be a consequence diminished control of a 5′ exonuclease (Hockemeyer et al., 2005).

More Than One Pathway for Telomere Protection

The results argue against models in which all telomere protection is simply based on the loading of one protective protein. Rather, different shelterin components have distinct as well as overlapping roles in preventing inappropriate DNA damage signaling and repair at chromosome ends (Figure 7). POT1b is required for the maintenance of a normal telomere terminus structure. Neither POT1a nor TRF2 have the ability to control this pathway when POT1b is absent. On the other hand, complete repression of DNA damage signaling at telomeres requires POT1a. POT1b is insufficient to fully protect telomeres in this regard although its contribution to this pathway is inferred from the more severe telomere damage phenotype of the DKO cells. TRF2 is also required for repression of the

telomere DNA damage signal although it remains to be determined whether its function is independent of POT1a/b. In contrast, the protection of telomeres from NHEJ involves a pathway that requires TRF2 but is largely independent of the POT1 paralogs. The simplest interpretation of these findings is that telomere protection is achieved through at least three distinct pathways: POT1b-dependent control of the terminus structure; repression of a DNA damage signal involving TRF2, POT1a, and POT1b; and TRF2-dependent repression of NHEJ. In addition, telomeres are protected from inappropriate homologous recombination, but the genetic requirements for this aspect of telomere function remain largely undefined (Wang et al., 2004).

Implications

The unusual divergence of mouse shelterin has implications for the use of mouse models for human telomere-related disease states. Deletion of essential telomerase components has allowed the establishment of mice with shortening telomeres that ultimately become dysfunctional and mimic aspects of telomere dysfunction in human cells (Blasco et al., 1997; Erdmann et al., 2004). These systems have been used to study the impact of telomere dysfunction on tumorigenesis, revealing that telomere dysfunction can limit tumor progression in some settings while promoting genome instability in others (Artandi et al., 2000; Greenberg et al., 1999; Maser and DePinho, 2002). Furthermore, the telomerase-knockout mouse has been used to model aspects of the human telomerase disease, dyskeratosis congenita (Armanios et al., 2005), and to study interactions between shortening telomeres and genetic defects such as Ataxia Telangiectasia and Werner syndrome (Laud et al., 2005; Qi et al., 2003; Wong et al., 2003). Similarly, we have used a mouse TRF2-knockout model to dissect the signaling pathway activated by dysfunctional telomeres (Celli and de Lange, 2005). Interpretation of these and other experiments rely on the assumption that mouse and human telomeres are structurally and functionally identical. The finding of an altered shelterin at mouse telomeres challenges this assumption. As more refined mouse models are developed, the potential pitfalls of working within the context of a different shelterin complex will have to be taken into account and the principles gleaned from work on mouse telomeres will require detailed verification in human cells.

EXPERIMENTAL PROCEDURES

Mice and MEFs with Altered POT1 Alleles

POT1a$^{8GEO/+}$ mice were generated from the Baygenomics clone RRA096. Gene-targeting constructs for POT1a and POT1b were generated using appropriate restriction fragments from BAC clones subcloned into pSL301 (Invitrogen) next to a DTA cassette. A STOP cassette (Jackson et al., 2001) flanked by FRT sites was introduced. The constructs also contained a puromycin resistance gene next to the STOP cassette and a neomycin resistance gene flanked by LoxP sites. A third LoxP site was introduced by inserting an oligonucleotide that also introduced a BamHI restriction site used for the analysis of targeting in ES cells. Targeted ES cell clones were injected into C57BL/6J blastocysts, and chimeric founders were crossed to C57BL/6J females. Mice were kept in a mixed 129/ C57BL/6J background. FLOXed alleles were generated by removing the STOP cassette using a FLPe deleter mouse stain (Jackson Labs). mTERC-deficient mice (Blasco et al., 1997) were obtained from R.A. DePinho and C.W. Greider. MEFs were isolated from a cross of a male POT1b$^{STOP/FLOX}$ mTERC$^{-/-}$ mouse and a female POT1b$^{FLOX/FLOX}$mTERC$^{+/-}$ mouse. Primary MEFs from E13.5 embryos were immortalized at passage 2 with pBabeSV40LT (a gift from G. Hannon). Cre was introduced using Hit&Run Cre-GFP (Silver and Livingston, 2001), pWZL-Cre, or Ad5 CMV Cre (Resource Center, The University of Iowa, Iowa City, IA) and deletion was monitored by PCR. POT1 proteins were stably knocked down in NIH3T3 cells using pSicoR-GFP vector technology (Ventura et al., 2004; a gift from T. Jacks).

ChIP, IF, and Immunoblotting

ChIPs were performed as described previously (Loayza and de Lange, 2003; Ye et al., 2004) with the difference that a probe for the BamHI repeat element (Fanning, 1983) was used to detect bulk genomic DNA. Immunoblots and IF for POT1a and POT1b were performed using the protocols described previously (Hockemeyer et al., 2005; Loayza and de Lange, 2003). POT1a antibodies 1220 and 1221 were raised in rabbits against a POT1a peptide representing amino acids 395–421. POT1b antibodies 1222 and 1223 were raised against a POT1b peptide representing amino acids 285–307. IF for γ-H2AX was performed using a mouse $\alpha-\gamma-$H2AX antibody (Upstate Biotechnology, Lake Placid, NY); 53BP1 FISH/IF staining was performed using a polyclonal rabbit anti human 53BP1 antibody, (Novus, [NB 100-304]) using the protocol developed by Sedivy and colleagues (Herbig et al., 2004). POT1a IF was performed using a mouse antibody against GST-POT1a fusion protein. POT1b IF was performed using a mouse antibody against GST-fused to POT1b (aa 1–342). TRF1 IF was performed with Ab 644 (Karlseder et al., 2003).

Analysis of Telomeric DNA

Mouse telomeric DNA was analyzed on CHEF gels using previously described protocols (Celli and de Lange, 2005). FISH for telomeric DNA was preformed as described (Celli and de Lange, 2005), with the exception that a FITC-TelC (FITC-OO-CCCTAACCCTAAACCCTAA, Applied Biosystems) probe was used to detect telomeric DNA.

Detailed Supplemental Experimental Procedures are available in the Supplemental Data.

Supplemental Data

Supplemental Data include Supplemental Experimental Procedures, five figures, and Supplemental References and can be found with this article online at http://www.cell.com/cgi/content/full/126/1/63/DC1/.

ACKNOWLEDGMENTS

We thank Sandy Chang for exchange of manuscripts after acceptance. We gratefully acknowledge Devon White for mouse husbandry and the RU and MSKCC Gene Targeting and Transgenic facilities for help in generating genetically modified mouse strains. Alan Li is thanked for assistance with genotyping. We thank Diego Loayza, Eros Lazzerini Denchi, Jeffrey Ye, Nadya Dimitrova, Kristina Hoke, and Giulia Celli for invaluable assistance with protocols and helpful discussion. Eric Brown, David Livingston, Tyler Jacks, David Tuveson, Greg Hannon, Ron DePinho, and Carol Greider are thanked for providing reagents and protocols. D.H. was supported by a Cancer Research Institute Predoctoral Emphasis Pathway in Tumor Immunology Grant and RU Graduate Program Funds. The Diplom thesis research of J.-P. D. was supported by the Studienstiftung des deutschen Volkes. This work was supported by grants from the National Institutes of

Health (AG16642 and GM49046) and the National Cancer Institute (CA76027).

Received: January 11, 2006
Revised: March 12, 2006
Accepted: April 28, 2006
Published: July 13, 2006

REFERENCES

Armanios, M., Chen, J.L., Chang, Y.P., Brodsky, R.A., Hawkins, A., Griffin, C.A., Eshleman, J.R., Cohen, A.R., Chakravarti, A., Hamosh, A., and Greider, C.W. (2005). Haploinsufficiency of telomerase reverse transcriptase leads to anticipation in autosomal dominant dyskeratosis congenita. Proc. Natl. Acad. Sci. USA *102*, 15960–15964.

Artandi, S.E., Chang, S., Lee, S.L., Alson, S., Gottlieb, G.J., Chin, L., and DePinho, R.A. (2000). Telomere dysfunction promotes non-reciprocal translocations and epithelial cancers in mice. Nature *406*, 641–645.

Bailey, S.M., Cornforth, M.N., Kurimasa, A., Chen, D.J., and Goodwin, E.H. (2001). Strand-specific Postreplicative Processing of Mammalian Telomeres. Science *293*, 2462–2465.

Baumann, P., and Cech, T.R. (2001). Pot1, the putative telomere end-binding protein in fission yeast and humans. Science *292*, 1171–1175.

Blasco, M.A., Lee, H.W., Hande, M.P., Samper, E., Lansdorp, P.M., DePinho, R.A., and Greider, C.W. (1997). Telomere shortening and tumor formation by mouse cells lacking telomerase RNA. Cell *91*, 25–34.

Celli, G., and de Lange, T. (2005). DNA processing not required for ATM-mediated telomere damage response after TRF2 deletion. Nat. Cell Biol. *7*, 712–718.

Chiang, Y.J., Kim, S.H., Tessarollo, L., Campisi, J., and Hodes, R.J. (2004). Telomere-associated protein TIN2 is essential for early embryonic development through a telomerase-independent pathway. Mol. Cell. Biol. *24*, 6631–6634.

d'Adda di Fagagna, F., Reaper, P.M., Clay-Farrace, L., Fiegler, H., Carr, P., Von Zglinicki, T., Saretzki, G., Carter, N.P., and Jackson, S.P. (2003). A DNA damage checkpoint response in telomere-initiated senescence. Nature *426*, 194–198.

de Lange, T. (2005). Shelterin: the protein complex that shapes and safeguards human telomeres. Genes Dev. *19*, 2100–2110.

Erdmann, N., Liu, Y., and Harrington, L. (2004). Distinct dosage requirements for the maintenance of long and short telomeres in mTert heterozygous mice. Proc. Natl. Acad. Sci. USA *101*, 6080–6085.

Fanning, T.G. (1983). Size and structure of the highly repetitive BAM HI element in mice. Nucleic Acids Res. *11*, 5073–5091.

Garvik, B., Carson, M., and Hartwell, L. (1995). Single-stranded DNA arising at telomeres in cdc13 mutants may constitute a specific signal for the RAD9 checkpoint. Mol. Cell. Biol. *15*, 6128–6138.

Greenberg, R.A., Chin, L., Femino, A., Lee, K.H., Gottlieb, G.J., Singer, R.H., Greider, C.W., and DePinho, R.A. (1999). Short dysfunctional telomeres impair tumorigenesis in the INK4a(delta2/3) cancer-prone mouse. Cell *97*, 515–525.

Griffith, J.D., Comeau, L., Rosenfield, S., Stansel, R.M., Bianchi, A., Moss, H., and de Lange, T. (1999). Mammalian telomeres end in a large duplex loop. Cell *97*, 503–514.

Herbig, U., Jobling, W.A., Chen, B.P., Chen, D.J., and Sedivy, J.M. (2004). Telomere shortening triggers senescence of human cells through a pathway involving ATM, p53, and p21(CIP1), but not p16(INK4a). Mol. Cell *14*, 501–513.

Hockemeyer, D., Sfeir, A.J., Shay, J.W., Wright, W.E., and de Lange, T. (2005). POT1 protects telomeres from a transient DNA damage response and determines how human chromosomes end. EMBO J. *24*, 2667–2678.

Horvath, M.P., Schweiker, V.L., Bevilacqua, J.M., Ruggles, J.A., and Schultz, S.C. (1998). Crystal structure of the Oxytricha nova telomere end binding protein complexed with single strand DNA. Cell *95*, 963–974.

Jackson, E.L., Willis, N., Mercer, K., Bronson, R.T., Crowley, D., Montoya, R., Jacks, T., and Tuveson, D.A. (2001). Analysis of lung tumor initiation and progression using conditional expression of oncogenic K-ras. Genes Dev. *15*, 3243–3248.

Karlseder, J., Broccoli, D., Dai, Y., Hardy, S., and de Lange, T. (1999). p53- and ATM-dependent apoptosis induced by telomeres lacking TRF2. Science *283*, 1321–1325.

Karlseder, J., Kachatrian, L., Takai, H., Mercer, K., Hingorani, S., Jacks, T., and de Lange, T. (2003). Targeted deletion reveals an essential function for the telomere length regulator Trf1. Mol. Cell. Biol. *23*, 6533–6541.

Laud, P.R., Multani, A.S., Bailey, S.M., Wu, L., Ma, J., Kingsley, C., Lebel, M., Pathak, S., DePinho, R.A., and Chang, S. (2005). Elevated telomere-telomere recombination in WRN-deficient, telomere dysfunctional cells promotes escape from senescence and engagement of the ALT pathway. Genes Dev. *19*, 2560–2570.

Lei, M., Podell, E.R., and Cech, T.R. (2004). Structure of human POT1 bound to telomeric single-stranded DNA provides a model for chromosome end-protection. Nat. Struct. Mol. Biol. *11*, 1223–1229.

Liu, D., Safari, A., O'Connor, M.S., Chan, D.W., Laegeler, A., Qin, J., and Songyang, Z. (2004). PTOP interacts with POT1 and regulates its localization to telomeres. Nat. Cell Biol. *6*, 673–680.

Loayza, D., and de Lange, T. (2003). POT1 as a terminal transducer of TRF1 telomere length control. Nature *424*, 1013–1018.

Maser, R.S., and DePinho, R.A. (2002). Connecting chromosomes, crisis, and cancer. Science *297*, 565–569.

Qi, L., Strong, M.A., Karim, B.O., Armanios, M., Huso, D.L., and Greider, C.W. (2003). Short telomeres and ataxia-telangiectasia mutated deficiency cooperatively increase telomere dysfunction and suppress tumorigenesis. Cancer Res. *63*, 8188–8196.

Silver, D.P., and Livingston, D.M. (2001). Self-excising retroviral vectors encoding the Cre recombinase overcome Cre-mediated cellular toxicity. Mol. Cell *8*, 233–243.

Smogorzewska, A., Karlseder, J., Holtgreve-Grez, H., Jauch, A., and de Lange, T. (2002). DNA Ligase IV-Dependent NHEJ of Deprotected Mammalian Telomeres in G1 and G2. Curr. Biol. *12*, 1635–1644.

Stansel, R.M., de Lange, T., and Griffith, J.D. (2001). T-loop assembly in vitro involves binding of TRF2 near the 3′ telomeric overhang. EMBO J. *20*, 5532–5540.

Takai, H., Smogorzewska, A., and de Lange, T. (2003). DNA damage foci at dysfunctional telomeres. Curr. Biol. *13*, 1549–1556.

van Steensel, B., Smogorzewska, A., and de Lange, T. (1998). TRF2 protects human telomeres from end-to-end fusions. Cell *92*, 401–413.

Veldman, T., Etheridge, K.T., and Counter, C.M. (2004). Loss of hPot1 function leads to telomere instability and a cut-like phenotype. Curr. Biol. *14*, 2264–2270.

Ventura, A., Meissner, A., Dillon, C.P., McManus, M., Sharp, P.A., Van Parijs, L., Jaenisch, R., and Jacks, T. (2004). Cre-lox-regulated conditional RNA interference from transgenes. Proc. Natl. Acad. Sci. USA *101*, 10380–10385.

Wang, R.C., Smogorzewska, A., and de Lange, T. (2004). Homologous recombination generates T-loop-sized deletions at human telomeres. Cell *119*, 355–368.

Wong, K.K., Maser, R.S., Bachoo, R.M., Menon, J., Carrasco, D.R., Gu, Y., Alt, F.W., and DePinho, R.A. (2003). Telomere dysfunction and Atm deficiency compromises organ homeostasis and accelerates ageing. Nature *421*, 643–648.

Yang, Q., Zheng, Y.L., and Harris, C.C. (2005). POT1 and TRF2 cooperate to maintain telomeric integrity. Mol. Cell. Biol. *25*, 1070–1080.

Ye, J.Z., Hockemeyer, D., Krutchinsky, A.N., Loayza, D., Hooper, S.M., Chait, B.T., and de Lange, T. (2004). POT1-interacting protein PIP1: a telomere length regulator that recruits POT1 to the TIN2/TRF1 complex. Genes Dev. *18*, 1649–1654.

Zhu, X.D., Niedernhofer, L., Kuster, B., Mann, M., Hoeijmakers, J.H., and de Lange, T. (2003). ERCC1/XPF Removes the 3′ Overhang from Uncapped Telomeres and Represses Formation of Telomeric DNA-Containing Double Minute Chromosomes. Mol. Cell *12*, 1489–1498.

Zubko, M.K., Guillard, S., and Lydall, D. (2004). Exo1 and Rad24 differentially regulate generation of ssDNA at telomeres of Saccharomyces cerevisiae cdc13–1 mutants. Genetics *168*, 103–115.

Cell, Volume *126*

Supplemental Data

Recent Expansion of the Telomeric

Complex in Rodents: Two Distinct POT1

Proteins Protect Mouse Telomeres

Dirk Hockemeyer, Jan-Peter Daniels, Hiroyuki Takai, and Titia de Lange

Rationale for the targeting strategy

Similar targeting strategies were used for POT1a and POT1b. For both genes, the third coding exon was deleted based on the considerations discussed here. For clarity, the details below only refer to POT1a.

According to the NCBI modelmaker tool (http://www.ncbi.nlm.nih.gov/mapview/modelmaker.cgi?QSTR=pot1&QUERY=uid(18408376)&taxid=10090&contig=NT_039340.6&gene=Pot1), deletion of the first two coding exons (exons 5 and 6 in the NCBI site) generates an N-terminally truncated POT1a protein lacking about one third of the first OB-fold (see Figure below). The truncation allele is predicted to start on an ATG in the 5'UTR, brought in frame with coding exon 3 by the normal splicing pattern of the POT1a mRNA. The Kozak score for this ATG is 0.403 and the resulting open reading frame is 607 aa. This ATG is closely followed by a second in-frame ATG with a score of 0.517, which better than the natural POT1a ATG (Kozak score of 0.497). Thus, truncation proteins of 600 and 607 aa might be generated if these ATGs are used in the context of deletion of the first two protein coding exons. These N-terminal deletions of POT1a will lack the ability to bind to single-stranded telomeric DNA but retain the ability to interact with the TPP1 component of shelterin. They are therefore expected to have a dominant negative effect, which has been documented for similar truncations of human POT1 (Loayza and de Lange, 2003). Furthermore, an N-terminal truncation allele of POT1a might be expected to affect POT1b function and vice versa.

Given these considerations, we opted for a targeting strategy that would allow conditional deletion of the third coding exon (exon 9 in the NCBI nomenclature) while preserving the first two coding exons. Upon deletion of exon 3, the protein initiated on the first ATG of POT1a will terminate early due to a frame-shift at position 41 which generates an in-frame stop codon four amino acids downstream. After this stop codon, there is no in-frame ATG until the methionine at aa position 112 in coding exon 4. Initiation on this ATG is predicted to yield a 528 aa truncation allele lacking DNA binding activity. As detailed above, such alleles are expected to act as dominant negative alleles. However, use of this ATG is rendered less likely since there is a favorable ATG upstream and therefore the generation of the 528 aa protein most likely requires reinitiation. The drawing below gives the amino acid and exon information and lists the Kozak score values for the pertinent ATGs as well as the length of the predicted open reading frames.

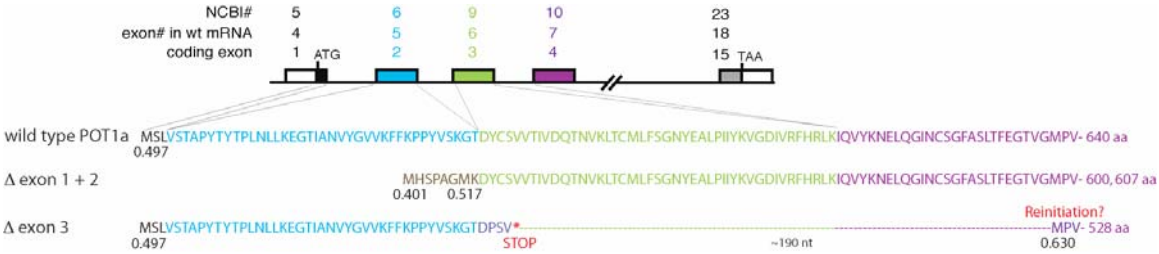
NCBI#
exon# in wt mRNA
coding exon
5
4
1
ATG
6
5
2
9
6
3
10
7
4
23
18
15
TAA
wild type POT1a
MSLVSTAPYTYTPLNLLKEGTIANVYGVVKFFKPPYVSKGTDYCSVVTIVDQTNVKLTCMLFSGNYEALPIIYKVGDIVRFHRLKIQVYKNELQGINCSGFASLTFEGTVGMPV- 640 aa
0.497
Δ exon 1 + 2
MHSPAGMKDYCSVVTIVDQTNVKLTCMLFSGNYEALPIIYKVGDIVRFHRLKIQVYKNELQGINCSGFASLTFEGTVGMPV- 600, 607 aa
0.401
0.517
Δ exon 3
MSLVSTAPYTYTPLNLLKEGTIANVYGVVKFFKPPYVSKGTDPSV*
Reinitiation?
MPV- 528 aa
0.497
STOP
~190 nt
0.630

Supplemental Experimental Procedures

Altered POT1 alleles

POT1a$^{8GEO/+}$ mice were generated from the Baygenomics clone RRA096 using protocols supplied by Baygenomics website (http://baygenomics.ucsf.edu/). Chimeras were generated by blastocyst injections of C57BL/6J blastocysts and founder chimeras were backcrossed to female C57BL/6J mice obtained from Jackson laboratory, USA. SA-β-galactosidase staining of E13.5 mouse embryos was performed as described on the Baygenomics website.

For gene-targeting of POT1a and POT1b, BAC clones of genomic DNA were isolated form the CT7 male CJ7/129SV BAC library (Research Genetics) using the first coding exons of POT1a and POT1b as probes. Appropriate restriction fragments (POT1a: HindIII/SacI fragment; POT1b XhoI/NheI fragment) were subcloned into pSL301 (Invitrogene) next to the negative selection (DTA) cassette. A STOP cassette (Jackson et al., 2001) flanked by FRT sites was introduced into the KpnI and NdeI sites for POT1a and –b, respectively. The constructs contained a puromycin resistance gene next to the STOP cassette and a neomycin resistance gene flanked by LoxP sites. A third LoxP site was introduced by inserting and oligonucleotide into a NheI and ApaI site for POT1a and POT1b, respectively. This oligo nucleotide introduced a BamHI restriction site used for the analysis of targeting in ES cells. The vector was linearized with SalI, and gene targeting was performed following standard techniques using the E14 ES cell line derived from 129P2/Ola. Genomic blotting with probes positioned outside of the targeting constructs were used to identify the diagnostic BamHI restriction fragment in correctly targeted ES cells. A probe specific for neo showed that there was only one integration event and confirmed the presence of the STOP cassette. ES cell clones that fulfilled these criteria were selected for C57BL/6J blastocyst injection and resulting chimeric founders were crossed to C57BL/6J females. Mice were kept in a mixed 129/ C57BL/6J mixed background. FLOXed alleles were generated by removing the STOP cassette using the 129S4/SvJaeSor-Gt(ROSA)26Sortm1(FLP1)Dym/J FLPe deleter mouse stain (Jackson Labs). mTERC deficient mice (Blasco et al., 1997) were obtained form R.A. DePinho and C.W. Greider. MEFs were isolated from a cross of a male POT1b$^{STOP/FLOX}$ mTERC-/- mice and a female POT1b$^{FLOX/FLOX}$mTERC$^{+/-}$ mice.

Genotyping

Genotyping PCRs were preformed using standard DNA isolation techniques and Takara Taq polymerase (Madison, WI, USA). POT1a wt PCR: 6-wtfw-1 CCAGCCTCCCCTCCACCAAGTC; 6-FRTbw-1 ACAAACCCACCCCGTCAGAGTAAG. POT1a FLOX PCR: 6-FRTfw-2 TGAGCCCAGAAAGCGAAGGAG; 6-FRTbw1 ACAAACCCACCCCGTCAGAGTAAG. POT1a ∆ex3 PCR: 6-allfw-2 CTTCCCTGTTTGCCCTCCTTTACT; 6-allbw-2 TTCCCCCTTTCATTTTCTTTTCTC. POT1b wt PCR: 17-wtfw-1 CGCTGGGGAGGGTATCGTAG; 17wtbw-1TCCCTGCCCTGACTTCCATC. POT1b FLOX PCR: 17wtfw-1 CGCTGGGGAGGGTATCGTAG; 6-FRTfw-2 TGAGCCCAGAAAGCGAAGGAG. POT1b ∆ex3 PCR: 17-allfw-1 GTTGCCCCTATCATCCTACACG; 17-FRTbw-2 TGTGTTGGGAGAGGAAGTGAAAGA. These PCRs were performed for 32 cycles (94°C for 45 s, 60°C for 45 s, 72°C for 60 s). POT1a and POT1b STOP PCR: 6-FRTfw-2 TGAGCCCAGAAAGCGAAGGAG and 6-Neobw-1 CCCCCTTCCCTGTTTGCCCTCCTT at 32 cycles (94°C for 30 s, 58°C for 30 s, 72°C for 60 s). Identity of the PCR products were confirmed by restriction endonuclease digestion and/or DNA sequencing.

Isolation and culturing of MEFs

Primary MEFs were obtained from E13.5 embryos using standard techniques and grown in DMEM containing 15% heat-inactivated fetal bovine serum (Gibco/Invitrogen), 100 U/ml penicillin (Sigma), 0.1 µg/ml streptomycin (Sigma), 2.0 mM L-glutamine (Gibco), 0.1 mM non-essential amino acids, 1 mM sodium pyruvate (Sigma) and 50 µM β-mercaptoethanol (Sigma). SV40 large T antigen immortalized MEFs were cultured in the same media without pyruvate and β-mercaptoethanol. MEFs were immortalized at passage 2 with pBabeSV40LT (a gift from G. Hannon) using the retroviral infection protocol given below.

Expression of Cre recombinase

Cre was introduced into immortalized MEFs using pMMPHit&Run Cre-GFP (Silver and Livingston, 2001), pWzl-Cre (containing the hygromycin resistance gene), or Ad5 CMV Cre (Resource center, The University of Iowa Carver College of Medicine GTVC, Iowa City, USA). For all experiments, Cre-mediated gene deletion was monitored by PCR. For retroviral gene delivery, 4 million Phoenix$_E$ cells were transfected with 15 µg of retroviral construct DNA using a standard calcium phosphate transfection protocol, changing the medium 6 hrs after transfection. Virus containing medium was collected at 48, 60, 72 and 84 hours post-transfection and used in 4 sequential infections of MEFs. Virus containing medium was passed through a 0.45 µm filter and supplemented with 4 µg/ml polybrene prior to infection. For adenoviral Cre delivery, 0.5 million SV40 transformed MEFs were infected in suspension with adenovirus at 0.8-1pfu/cells. The effective adenoviral titer was determined in GFP-LacZ 293T reporter cells ((Brown and Baltimore, 2003); a gift from E. Brown). The infection was repeated after 6 hours and 12 hours later the medium was replaced with virus free medium. Using this protocol re-adherence of the cells was efficient (>95%) and cell death was minimal prior the deletion mediated by the Cre. Cre-mediated deletion efficiency was >80% at 78 hours post infection.

shRNA constructs

POT1 proteins were stably knocked down in NIH3T3 cells using pSicoR-GFP vector technology ((Ventura et al., 2004); a gift from T. Jacks). The following target sequences were cloned into pSico and confirmed by DNA sequencing: a1: GCATCACTATGGATGTAAA; a* (inactive): GGAACTCCCAAATAAAGTA; a3: GCATTTCTCTACAACATTA; b1: GCAGCTGCTTTGAAGATTA; b2: GGAGTGTCATTTCTCCTAA; b3: GGAGAAGGGTGATCCTGTA. Three days before the infection, 293T cells were transfected with 3.5 µg of each helper plasmid pMDLg/RRE, pRSV-rev and pCMV-VSVG and 7 µg of lentiviral vector per 10 cm dish, using calcium phosphate transfection. 72 hrs after changing the medium on the transfected cells, half of the virus-containing medium supplemented with 4 µg/ml polybrene was used to infect 75,000 NIH3T3 cells. After 3 hrs, the infection was repeated and 3 hrs later, the virus containing medium was replaced by pre-warmed fresh medium. The infection efficiency was >90% as determined using lentiviral vectors carrying the GFP gene (pSicoR-GFP and derivates) and quantification of cells that exhibited GFP fluorescence at 48 hrs after infection. Cells used in ChIP analysis were generated by two rounds of infection with the indicated lenti-viruses separated by approximately one week of culture.

ChIP, IF, and immunobloting

ChIPs were performed as described previously (Loayza and de Lange, 2003; Ye et al., 2004) with the difference that a probe for the BamHI repeat element (Fanning, 1983) was used to detect bulk genomic DNA. Immunoblots and IF for POT1a and POT1b were performed using the protocols described previously (Hockemeyer et al., 2005; Loayza and de Lange, 2003). For IF, one million cells were plated on 12 mm cover slips and

grown for 24 hrs. All following steps were performed at RT. Cells were rinsed in PBS, fixed for 10 min in 2% formaldehyde in PBS, washed twice in PBS for 5 min and permeabilized in 0.5% NP-40 (Nonidet P-40 Substitute) in PBS (v/v) for 10 min, and then washed twice in PBS for 5 min. Non-specific interactions were blocked with PBG (1% BSA, 0.2% cold fish gelatin in PBS) for 30 min, before incubation in primary antibody in PBG for 2 hours. Cover slips were washed 3 times with PBG for 5 min and incubated with secondary antibodies in PBG (donkey anti-rabbit IgG-RRX conjugated (1:250), donkey anti-mouse IgG-Alexa488 conjugated (1:250)) for 45 min. After two washes in PBG, in 100 ng/ml DAPI in PBS, and in PBS for 5 min each, cover slips were mounted on microscope slides and analyzed using a Zeiss Axioplan II (Thornwood, CA, USA) fluorescence microscope in combination with a Hamamatsu digital camera (C474295) (Bridgewater, MA, USA). Cells were randomly chosen by screening the slides with a ZEISS Plan Apochroma 63X/1.40 Oil DIC objective in the DAPI channel of the fluorescence microscope. For all dual IF experiments, bleed-through controls were performed by leaving out one of the two primary antibodies.

POT1a antibodies 1220 and 1221 were raised in rabbits against a POT1a peptide representing amino acids 395-421. POT1b antibodies 1222 and 1223 were raised against a POT1b peptide representing amino acids 285-307. IF for γ-H2AX was performed using a mouse α–γ–H2AX antibody (Upstate Biotechnology, Lake Placid, NY); 53BP1 FISH/IF staining was performed using a polyclonal rabbit anti human 53BP1 antibody, (Novus, (NB 100-304)) using the protocol developed by Sedivy and colleagues (Herbig et al., 2004). POT1a IF was performed using an antibody raised in mice against recombinant GST-tagged full-length POT1a protein. POT1b IF was performed using an antibody raised in mice against GST-tagged POT1b protein from amino acid 1 to 342 (the C-terminus contained the additional amino acids SKPFSSVVTDT). TRF1 IF was performed with Ab 644 (Karlseder et al., 2003)**.**

Analysis of telomeric DNA

Mouse telomeric DNA was analyzed on CHEF gels using previously described protocols (Celli and de Lange, 2005) using 0.5 million MEFs or 0.75 million cells from liver, kidney or spleen. The CHEF gel was dried on a gel dryer at RT, briefly rinsed in water and then pre-hybridized in 25 ml Church Mix (0.5M sodium phosphate, pH 7.2, 1mM EDTA, 0.7% SDS, 0.1% BSA) in a sealed bag for 1 hr at 50°C with agitation. The gel was hybridized with an end-labeled $[CCCTAA]_4$ oligonucleotide (50 ng) in 25 ml in Church mix at 50°C overnight. The gel was washed at 50°C in 4X SSC 0.1% SDS and exposed on a phosphoimager screen over night. The next day, the DNA was denatured in situ by incubating the gel for 30 min in denaturing solution (1.5 M NaCl, 0.5 M NaOH) and twice for 15 min in neutralizing solution (3 M NaCl, 0.5M Tris-HCl, pH 7.0). After rinsing for 3 min with ddH2O, the gel was pre-hybridized in 25 ml Church Mix at 55°C for 1 hr and hybridized with the same probe at 55°C o/n. The gel was then washed as above at 55°C and exposed for 2 hrs on a phosphoimager screen. Signals were quantified using ImageQuant software (Molecular Dynamics). The relative overhang signal is determined by the ratio between the native signal and signal in the same lane after denaturation.

Senescence associated β-galactosidase staining

For the SA-β-galactosidase assay (Dimri et al., 1995)**,** 10^5 cells were plated on a 6-well cell culture dish and 48 hrs later, the cells were washed twice in PBS for 5 min. The cells were fixed for 3 min in 2% formaldehyde and 0.2% glutaraldehyde in PBS and washed twice in PBS for 5 min. The staining reaction was performed with 3 ml staining solution (1 mg/ml 5-bromo-4-chloro-3-indolyl β-D-galactoside (X-Gal), 40 mM citric acid/sodium

phosphate, pH 6.0, 5 mM potassium ferrocyanide, 5 mM potassium ferricyanide, 150 mM NaCl, 2 mM $MgCl_2$) at 37°C for 8 to 14 hrs in the dark. Cells were washed twice with PBS and photographed.

FACS analysis

For FACS analysis, 10^6 cells were plated on 10 cm cell culture dishes and grown for 24 hrs. BrdU was added directly to the culture medium to a final concentration of 10 µM 60 min prior harvesting. Cells were collected, washed in PBS, and fixed in ice cold 70% ethanol for 30 min while mixing on ice. Cells were recovered by centrifugation and the DNA was denatured in 1 ml of 2N HCl in 0.5% Triton X-100 (v/v) added drop wise while mixing. After 30 min at rt, cells were recovered by centrifugation and samples were neutralized with 1 ml of 0.1 M sodium-tetraborate, pH 8.5. Cells were washed once with 0.5% BSA in PBS and re-suspended in 100 µl of 0.5% BSA in PBS. 10 µl of FITC-conjugated anti BrdU antibody (Becton Dickinson) was added and samples were incubated for 30 min at rt in the dark. Cells were washed twice with 0.5% BSA in PBS and re-suspended in 0.4 ml 0.5% BSA in PBS containing 5 µg propidium-iodide and 100 µg RNAseA per ml. The samples were analyzed on a FACScalibur flow cytometer (Becton Dickinson). Data analysis was performed using FlowJo software.

Telomere fluorescence *in situ* hybridization (FISH) on metaphase spreads.

FISH for telomeric DNA was preformed as described (Celli and de Lange, 2005), with the exception that a FITC-TelC (FITC-OO-CCCTAACCCTAAACCCTAA, Applied Biosystems) probe was used to detect telomeric DNA.

RT-PCR

RT-PCR was performed using a mouse cDNA panel form Research Genetics. cDNA was amplified using standard PRC techniques. POT1a primers: fw: TGGTTTCAACAGCTCCCTATA, bw:CCCTACAGTCCCTTCAAATG; POT1b primers: fw:CGGCCCCAGTAGCACCTTCTAC, bw:TCTCTTGCTTAAAGTACGCAG. RT-PCR was performed using the oligo-dT ThermoScript RT-PCR system, (Invitrogen). RNA was isolated from approximately 10^6 cells using Qiagene RNAeasy kit. 1 µg RNA was reverse transcribed using the thermoScript RT-PCR system (Invitrogen,USA) using oligo dT priming and the protocol provided by the manufacturer. To detect the recombined POT1a locus, fw: TGGTTTCAACAGCTCCCTATA and bw: CTTAGAAAGCATCCAACCTCG were used as primers.

Supplemental Figures

Supplemental Figure 1. Hockemeyer et al.

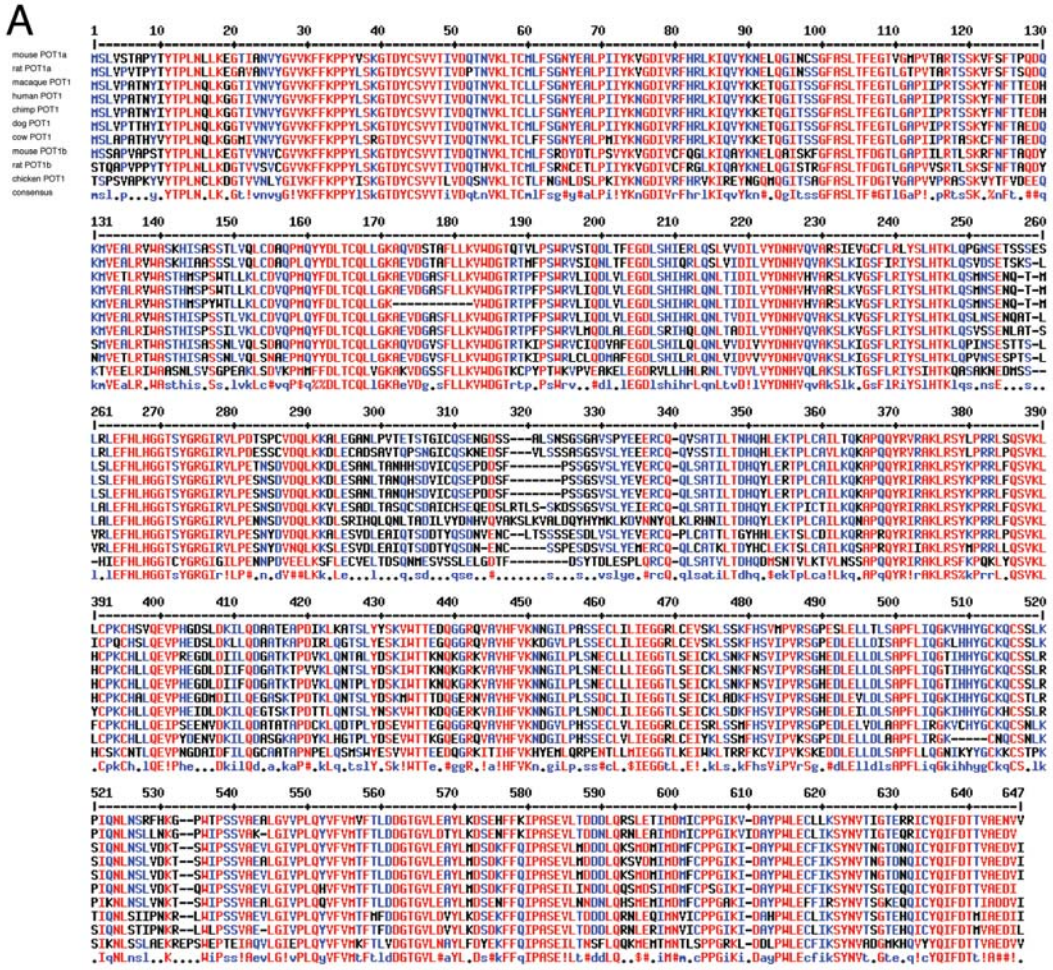

Supplemental Figure 1. Hockemeyer et al.

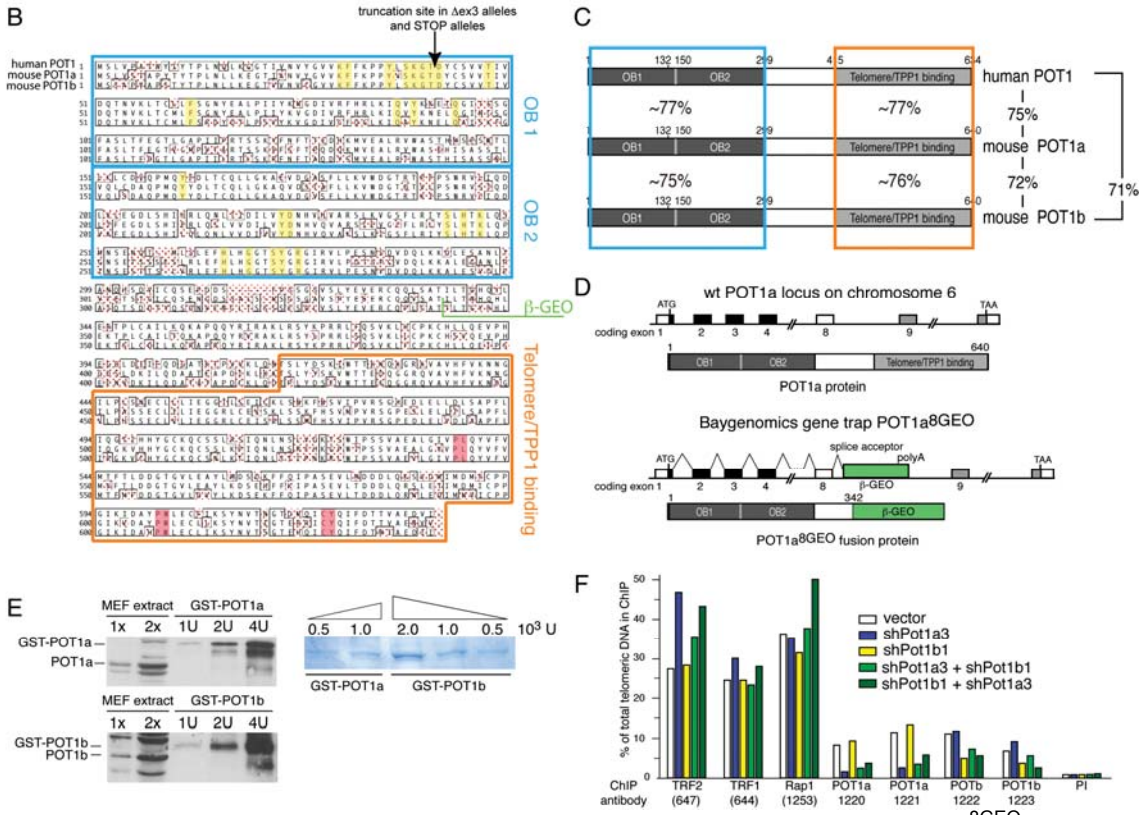

Supplemental Figure 1. Comparison of POT1 proteins, details of the POT1a^{8GEO} allele, and quantification of POT1a/b ChIP

(A) Alignments of the POT1 proteins of Mus musculus (mouse), Rattus norvegicus (rat), Homo sapiens (human), Pan troglodytes (chimpanzee), Canis familiaris (dog, boxer), Gallus gallus (chicken), and Bos taurus (cow). For part of the sequences (dog POT1, rat POT1b, and cow POT1) no EST information was available. These POT1 sequences were derived from BLAST searches of genomic DNA and spliced together based on identification of exon-intron boundaries using the human POT1 sequence as a guide. Alignments were generated by CLUSTALW using the Multialin website (http://prodes.toulouse.inra.fr/multalin/) and default setting for all parameters. Identical amino acids in red; similar amino acids in blue.

(B) Alignment of mouse POT1a and POT1b with human POT1 showing sequence identifies in functional domains and landmarks relevant to the altered mouse alleles. Identical amino acids are boxed black. Inferred OB-folds are boxed blue and the putative TPP1 interaction domains are boxed in yellow. Amino acids known from the crystal structure of human POT1 essential for DNA binding (Lei et al., 2004) are shaded yellow and amino acids known in human POT1 to be essential for the interaction with TPP1 (Hockemeyer et al., 2005; Loayza and de Lange, 2003; Veldman et al., 2004; Yang et al., 2005; Ye et al., 2004; Liu et al., 2004) are shaded red. Indicated are the truncation sites in POT1a and POT1b STOP alleles, POT1a and POT1b Δex3 alleles and the truncation site of POT1a in the POT1a^{8GEO} allele.

(C) Schematic overview of sequence similarity between hPOT1, POT1a and POT1b. Boxes as in (B).

(D) Schematic representation of the POT1a^{8GEO} allele. Shown are the wt POT1a locus on chromosome 6 and a schematic of the wt POT1a protein. Below the POT1a locus of

Baygenomics clone RRA096 is shown and a schematic overview of the truncated POT1a^{8GEO} protein.
(E) Quantitative analysis of expression levels of POT1a and POT1b. POT1a and POT1b signals obtained in MEF extract were compared to signals obtained with identical amounts of recombinant GST-POT1a and GST-POT1b fusion protein. Loading of equal amounts ("units") for the two GST fusion proteins was based on Coomassie staining as shown on the right.
(F) Bargraph of quantification of ChIP analysis show in Figure 1G.

Supplemental Figure 2. Hockemeyer et al.

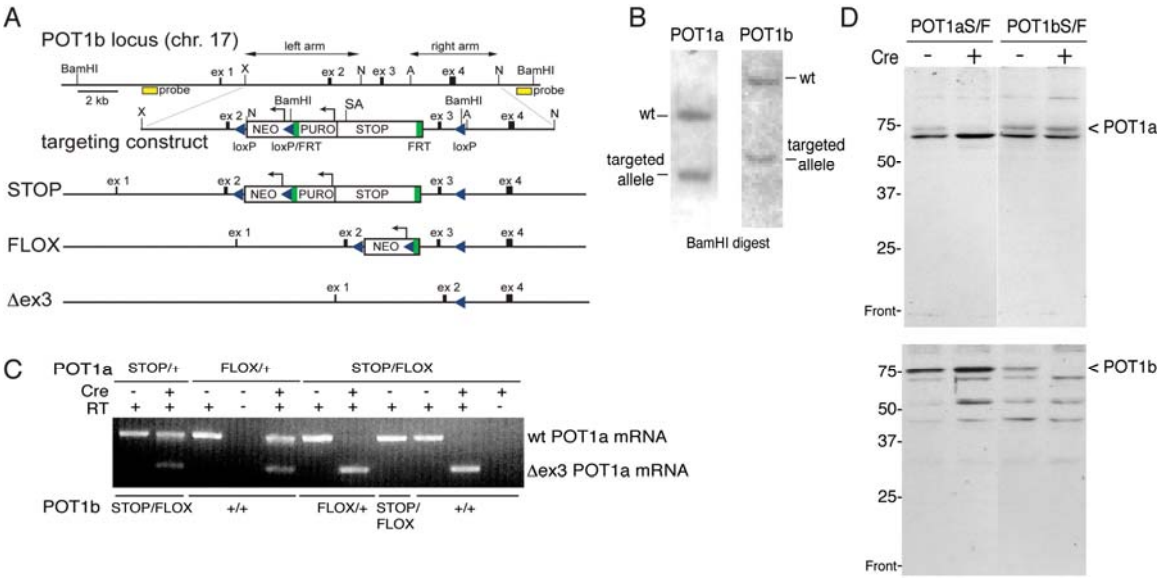

Supplemental Figure 2. Targeting of POT1a and POT1b
(A) Conditional knockout strategy used to target the POT1b gene. Given are the genomic locus on mouse chromosome 17 containing the coding exons 1-4 of the POT1b gene, the targeting construct, and the POT1b alleles generated. Yellow boxes: probes used for genotyping by genomic blotting of BamHI digested DNA (see Suppl. Fig. 2B); green boxes: FRT sites; blue: LoxP sites; SA: splice acceptor of the STOP cassette.
(B) Autoradiogram of genomic blotting analysis of BamHI digested DNA from ES-cells targeted with POT1a targeting construct (left panel) and POT1b (right panel) using the probes indicated in Fig. 2 and panel A (above) located proximal to exon 3.
(C) RT-PCR analysis of POT1a mRNA isolated from MEFs with the indicated genotypes after infection with pWzl-Cre or control vector and 4 days of selection.
(D) Immunoblot for POT1a and POT1b in control cells and after Cre-mediated deletion. Note that no new lower MW products are detected after Cre treatment.

Supplemental Figure 3. Hockemeyer et al.

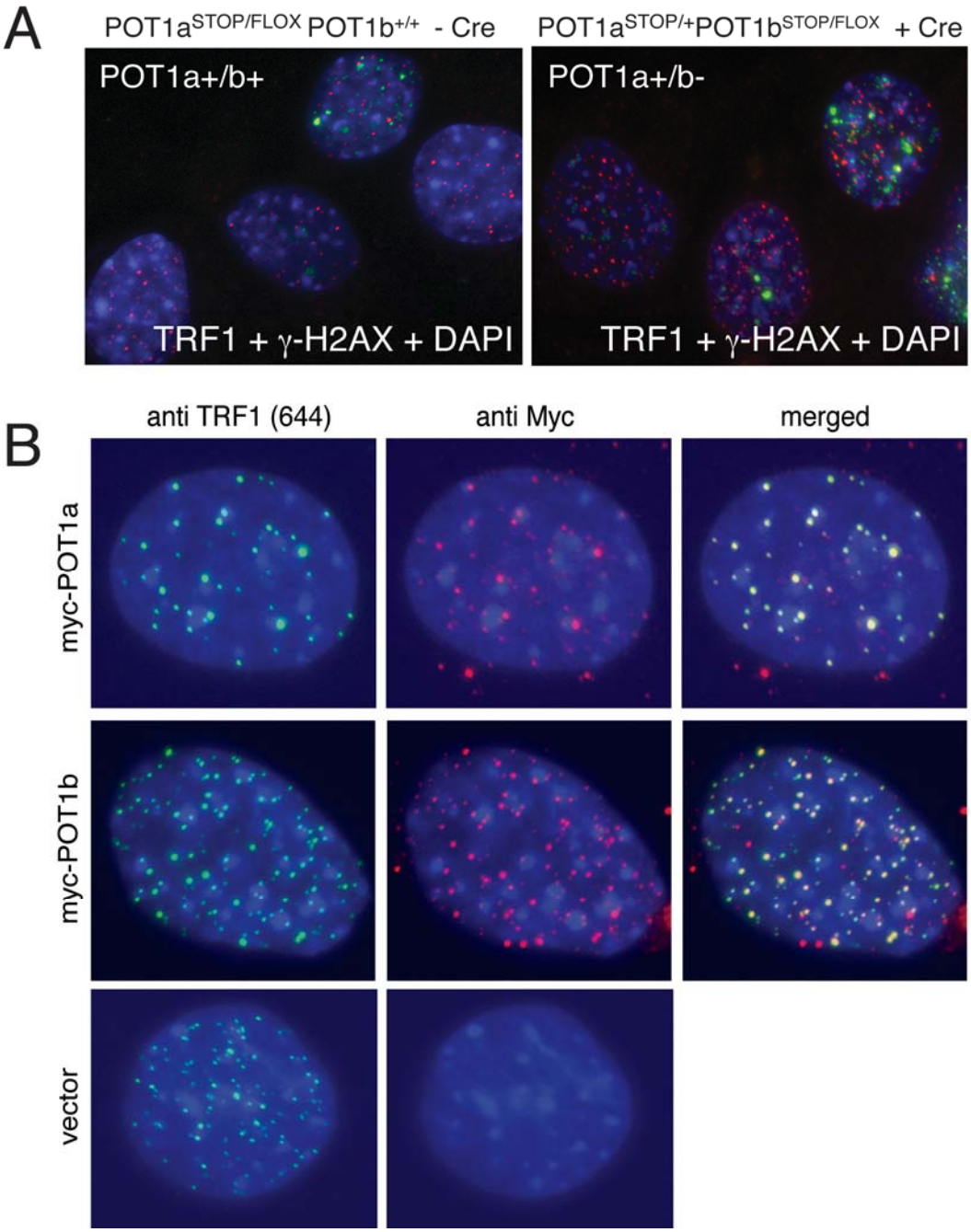

Supplemental Figure 3. TIF analysis on POT1b deficient cells and analysis of POT1a and POT1b proteins used for the suppression of the DNA damage response.
(A) TIF analysis as shown in Figure 3 (panel A) using MEFs with the indicated genotypes and Cre infection.
(B) Myc IF showing telomeric localization for exonously expressed myc-POT1a and myc-POT1b. MEFs were infected with the indicated retroviruses and processed for IF (myc, red) and TRF1 (green).

Supplemental Figure 4. Hockemeyer et al.

A

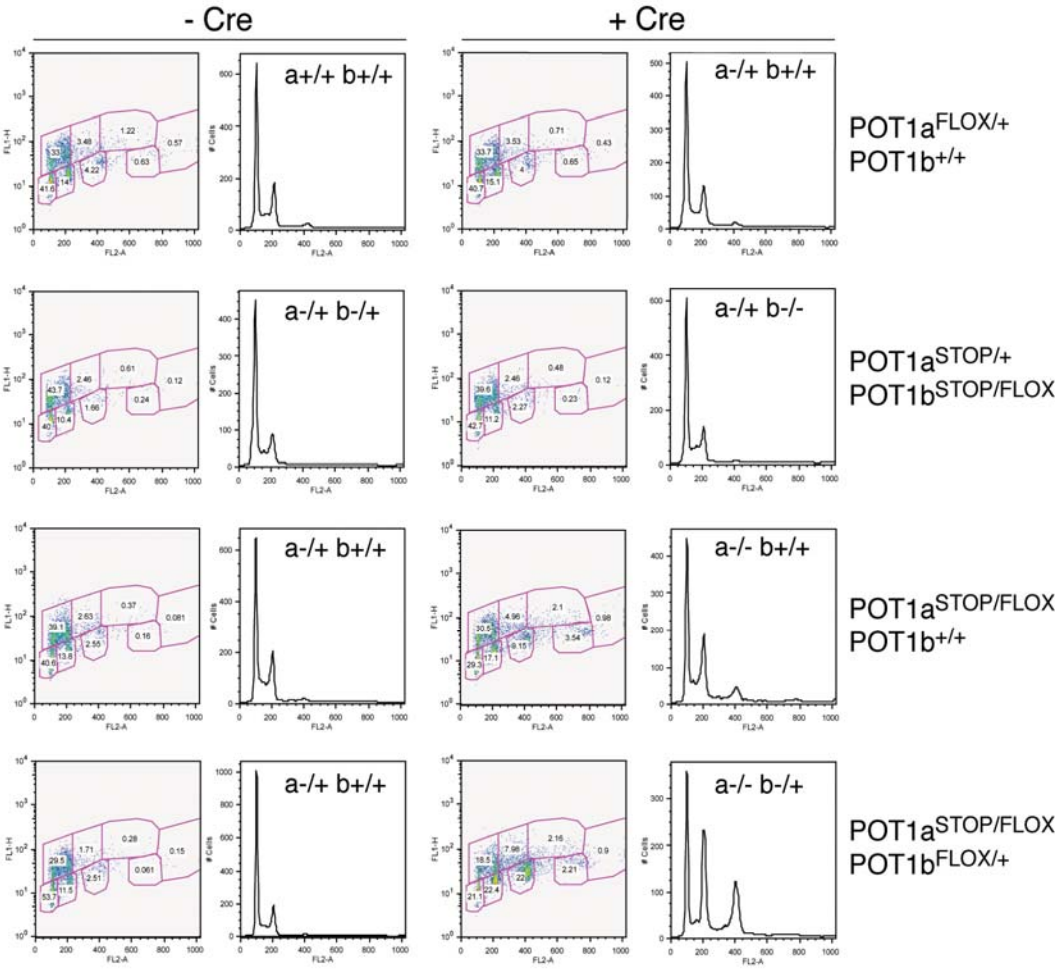

B

Genotype	Cre	POT1a status	POT1b status	Metaphases analyzed	Metaphases w/ diplo-chromosomes (%)
POT1a$^{FLOX/+}$ POT1b$^{+/+}$	-	+/+	+/+	54	2 (3.7%)
	+	-/+	+/+	50	1 (2%)
POT1a$^{STOP/+}$ POT1b$^{STOP/FLOX}$	-	-/+	-/+	59	3 (5%)
	+	-/+	-/-	51	1 (2%)
POT1a$^{STOP/FLOX}$ POT1b$^{+/+}$	-	-/+	+/+	54	2 (3.7%)
	+	-/-	+/+	63	11 (17%)
POT1a$^{STOP/FLOX}$ POT1b$^{STOP/FLOX}$	-	-/+	-/+	53	1 (1.9%)
	+	-/-	-/-	69	12 (17%)

Supplemental Figure 4. Cell cycle profile changes after deletion of POT1a or POT1b
(A) FACS profiles MEFs with the indicated genotypes and BrdU incorporation as in Figure 5 panels C and D.
(B) Frequency of diplochromosome-containing metaphases in MEFs with the indicated genotypes. Metaphases were generated as in Figure 5.

Supplemental Figure 5. Hockemeyer et al.

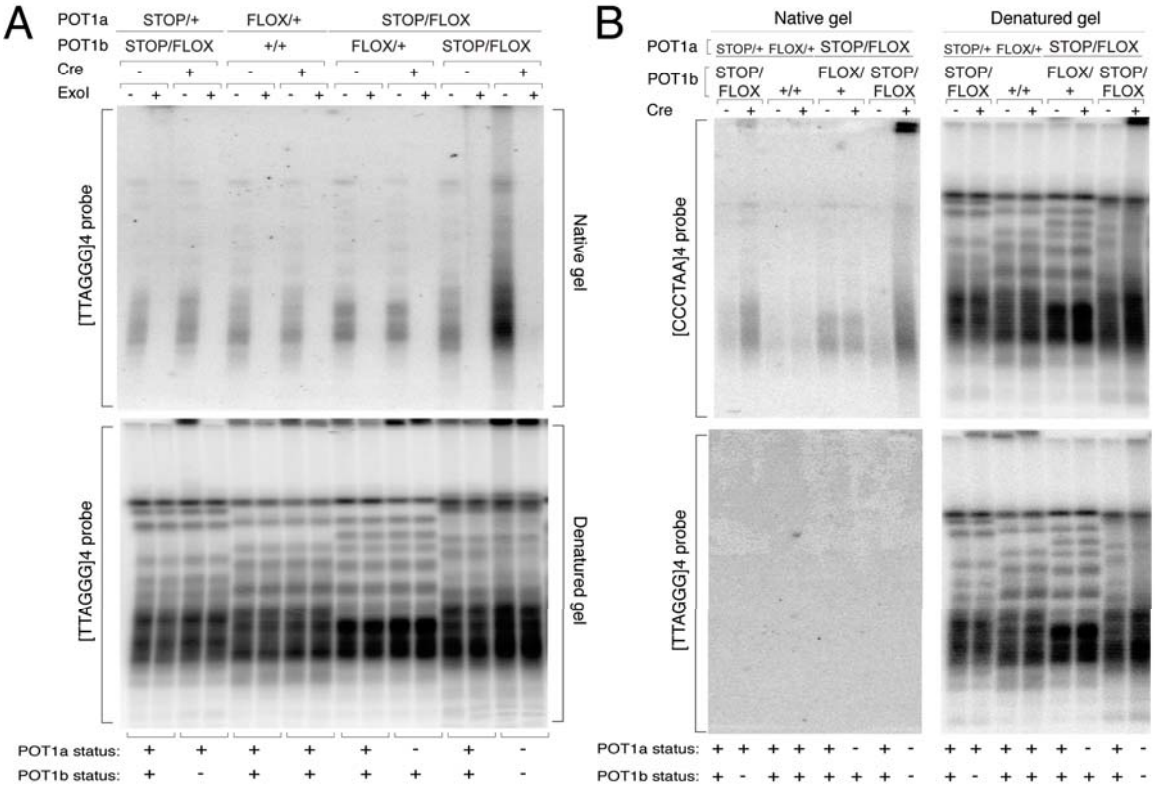

Supplemental Figure 5. ExoI and C-strand control experiments for extended overhang phenotype of POT1b deficiency.
(A) In-gel hybridization analysis on DNA from MEFs with the indicated genotypes treated as in Figure 6. Before digest of genomic DNA plugs were incubated with ExoI nuclease as indicated. Top panel shows the native overhang signal, bottom panel shows the denatured total telomeric DNA.
(B) In-gel hybridization of MEFs with the indicated genotypes treated as in Figure 6. Top panel: the single-stranded and total telomeric DNA signals obtained with a $[CCCTTA]_4$ probe. Bottom panel: the single-stranded and total telomeric DNA signals obtained with a $[TTAGGG]_4$ probe.

Supplemental References

Blasco, M. A., Lee, H. W., Hande, M. P., Samper, E., Lansdorp, P. M., DePinho, R. A., and Greider, C. W. (1997). Telomere shortening and tumor formation by mouse cells lacking telomerase RNA. Cell *91*, 25-34.

Brown, E. J., and Baltimore, D. (2003). Essential and dispensable roles of ATR in cell cycle arrest and genome maintenance. Genes Dev *17*, 615-628.

Celli, G., and de Lange, T. (2005). DNA processing not required for ATM-mediated telomere damage response after TRF2 deletion. Nat Cell Biol *7*, 712-718.

Dimri, G. P., Lee, X., Basile, G., Acosta, M., Scott, G., Roskelley, C., Medrano, E. E., Linskens, M., Rubelj, I., Pereira-Smith, O., and et al. (1995). A biomarker that identifies senescent human cells in culture and in aging skin in vivo. Proc Natl Acad Sci U S A *92*, 9363-9367.

Fanning, T. G. (1983). Size and structure of the highly repetitive BAM HI element in mice. Nucleic Acids Res *11*, 5073-5091.

Herbig, U., Jobling, W. A., Chen, B. P., Chen, D. J., and Sedivy, J. M. (2004). Telomere shortening triggers senescence of human cells through a pathway involving ATM, p53, and p21(CIP1), but not p16(INK4a). Mol Cell *14*, 501-513.

Hockemeyer, D., Sfeir, A. J., Shay, J. W., Wright, W. E., and de Lange, T. (2005). POT1 protects telomeres from a transient DNA damage response and determines how human chromosomes end. EMBO J. *24*, 2667-2678.

Jackson, E. L., Willis, N., Mercer, K., Bronson, R. T., Crowley, D., Montoya, R., Jacks, T., and Tuveson, D. A. (2001). Analysis of lung tumor initiation and progression using conditional expression of oncogenic K-ras. Genes Dev *15*, 3243-3248.

Karlseder, J., Kachatrian, L., Takai, H., Mercer, K., Hingorani, S., Jacks, T., and de Lange, T. (2003). Targeted deletion reveals an essential function for the telomere length regulator Trf1. Mol Cell Biol *23*, 6533-6541.

Lei, M., Podell, E. R., and Cech, T. R. (2004). Structure of human POT1 bound to telomeric single-stranded DNA provides a model for chromosome end-protection. Nat Struct Mol Biol *11*, 1223-1229.

Liu, D., Safari, A., O'Connor, M. S., Chan, D. W., Laegeler, A., Qin, J., and Songyang, Z. (2004). PTOP interacts with POT1 and regulates its localization to telomeres. Nat Cell Biol *6*, 673-680.

Loayza, D., and de Lange, T. (2003). POT1 as a terminal transducer of TRF1 telomere length control. Nature *424*, 1013-1018.

Silver, D. P., and Livingston, D. M. (2001). Self-excising retroviral vectors encoding the Cre recombinase overcome Cre-mediated cellular toxicity. Mol Cell *8*, 233-243.

Veldman, T., Etheridge, K. T., and Counter, C. M. (2004). Loss of hPot1 function leads to telomere instability and a cut-like phenotype. Curr Biol *14*, 2264-2270.

Ventura, A., Meissner, A., Dillon, C. P., McManus, M., Sharp, P. A., Van Parijs, L., Jaenisch, R., and Jacks, T. (2004). Cre-lox-regulated conditional RNA interference from transgenes. Proc Natl Acad Sci U S A *101*, 10380-10385.

Yang, Q., Zheng, Y. L., and Harris, C. C. (2005). POT1 and TRF2 cooperate to maintain telomeric integrity. Mol Cell Biol *25*, 1070-1080.

Ye, J. Z., Hockemeyer, D., Krutchinsky, A. N., Loayza, D., Hooper, S. M., Chait, B. T., and de Lange, T. (2004). POT1-interacting protein PIP1: a telomere length regulator that recruits POT1 to the TIN2/TRF1 complex. Genes Dev *18*, 1649-1654.